Soil Dynamics and Earthquake Engineering 80 (2016) 225–240

Contents lists available at ScienceDirect

Soil Dynamics and Earthquake Engineering

journal homepage: www.elsevier.com/locate/soildyn

Estimation of rocking and torsion associated with surface waves extracted from recorded motions

Kristel C. Meza-Fajardo [a,*], Apostolos S. Papageorgiou [b]

[a] Department of Civil Engineering, Universidad Nacional Autónoma de Honduras, Tegucigalpa, Honduras
[b] Department of Civil Engineering, University of Patras, GR-26500 Patras, Greece

ARTICLE INFO

Article history:
Received 1 April 2015
Received in revised form
23 October 2015
Accepted 29 October 2015
Available online 21 November 2015

Keywords:
Ground motion variability
Wave identification
Time–frequency analysis
Angular displacements
Phase velocity spectrum
Cross-spectrum analysis
Rocking
torsion

ABSTRACT

By exploiting the capability of identifying and extracting surface waves existing in a seismic signal, we can proceed to estimate the angular displacement (rotation about the horizontal axis normal to the direction of propagation of the wave; rocking) associated with Rayleigh waves as well as the angular displacement (rotation about the vertical axis; torsion) associated with Love waves.

For a harmonic Rayleigh (Love) wave, rocking (torsion) would be proportional to the harmonic vertical (transverse horizontal) velocity component and inversely proportional to the phase velocity corresponding to the particular frequency of the harmonic wave (a fact that was originally exploited by Newmark (1969) [15] to estimate torsional excitation). Evidently, a reliable estimate of the phase velocity (as a function of frequency) is necessary. As pointed out by Stockwell (2007) [17], because of its absolutely referenced phase information, the S-Transform can be employed in a cross-spectrum analysis in a local manner. Following this suggestion a very reliable estimate of the phase velocity may be obtained from the recordings at two nearby stations, after the dispersed waves have been identified and extracted. Synthesis of the abovementioned harmonic components can provide a reliable estimate of the rocking (torsional) motion induced by an (extracted) Rayleigh (Love) wave.

We apply the proposed angular displacement estimation procedure for two well recorded data sets: (1) the strong motion data generated by an aftershock of the 1999 Chi-Chi, Taiwan earthquake and recorded over the Western Coastal Plain (WCP) of Taiwan, and (2) the strong motion data generated by the 2010 Darfield, New Zealand earthquake and recorded over the Canterbury basin. The former data set is dominated by basin-induced Rayleigh waves while the latter contains primarily Love waves.

1. Introduction

Differential ground motion associated with the propagation of waves can potentially be an important factor in causing earthquake related ground failure and damage to extended structures. Furthermore, the angular displacement components (rocking and torsion) of ground motion may significantly contribute to the response and damage of structures (e.g., [15,11], just to refer to a couple of the pioneering works; rotational ground motion was the subject of a 2009 special issue of the *Bulletin of the Seismological Society of America* (No. 99, 2B)). In earthquake engineering, recognition that angular displacement components of strong motion may contribute significantly to the response of structures started to appear around the 1960's [19]. It was Newmark [15] who first developed a rational basis for determining the torsional earthquake effects in symmetrical buildings arising from a traveling wave propagating with a constant velocity. Hart et al. [8] attributed a large part of the torsional response of high-rise buildings during the 1971 San Fernando, California, earthquake to the rotational components of the ground motion, while Bycroft [3] associated the differential longitudinal motion, responsible for the collapse of bridges during the 1971 San Fernando earthquake and 1978 Miyagi-Ken-Oki, Japan, earthquake with the rotational components of ground motion. Trifunac et al. [20] discussed the distribution of inferred peak surface strains during the 1994 Northridge, CA, earthquake, and attributed the collapse of bridges to longitudinal differential ground motions. The dynamic strain field in the near-fault region of the above earthquake was investigated also by Gomberg [7] who proposed a method for estimating complete time varying strains from commonly available three-component single station seismic data. Finally, Huang [9] reported that large rotational motions, excited by the 1999 Chi-

* Corresponding author.
E-mail addresses: kristelmeza@unah.edu.hn (K.C. Meza-Fajardo), papaga@upatras.gr (A.S. Papageorgiou).

http://dx.doi.org/10.1016/j.soildyn.2015.10.017
0267-7261/

Chi, Taiwan earthquake, were inferred from a dense acceleration array near the northern end of the rupture fault where large surface slips along the fault were observed.

Angular displacement components of strong motion always accompany the translational displacement components induced by seismic waves. However, while the latter are measured directly in the field using commercially available sensors (accelerographs), the former are estimated approximately from the translational records, as there are currently no commercially available sensors to measure 'point rotations' (for a brief history of the development of rotation seismographs see [6]). Newmark, in his 1969 seminal paper, started with the 'point rotation' about a vertical axis expressed by space derivatives of displacements (as demanded by continuum mechanics) and eventually expressed it in terms of the ratio of the transverse (to the direction of propagation) component of translational horizontal velocity divided by an 'average' (i.e., independent of frequency) apparent horizontal phase velocity. This type of analysis is exact for plane harmonic waves and can be extended to consider not only rotation about a vertical axis (i.e., torsion) but also rotation about a horizontal axis (i.e., rocking), as demonstrated by Trifunac [18] (see also [21]). More importantly, it provides a single-station procedure to estimate 'point rotations' from common records of translational motion. The key parameter of the procedure is an appropriate selection of the above-mentioned 'average' apparent horizontal phase velocity, say c_{app} . In a ground breaking paper Bouchon and Aki [2] simulated numerically the rupturing of a fault embedded in a layered half-space and computed the field of differential motions (strains) in the region surrounding the rupturing fault. By comparing waveforms of appropriate components of differential motion with appropriate components of translational velocity, these authors confirmed Newmark's [15] result. Furthermore, they were able to estimate appropriate values for the parameter c_{app}. They observed that while in the immediate vicinity of the fault, c_{app} is controlled by the rupture velocity of the fault, elsewhere c_{app} was controlled by the basement rock shear-wave velocity (i.e., the shear-wave velocity of the medium/layer that contains the source) and not by the near-surface velocities. The latter observation is in agreement with results obtained earlier by Luco and Sotiropoulos [12] who demonstrated that the phase velocity of the ground motion produced by a point of shear dislocation, a few kilometers away from the source, is of the order of the shear-wave velocity in the source layer.

The above results and conclusions make very good sense (and are intuitively appealing), as far as body waves are concerned. However, when the discussion focuses on dispersive surface waves, especially those induced by the presence of sedimentary basins, then, the value of the parameter c_{app} is frequency dependent and depends on the structure/stratification/geometry of the sedimentary deposits. Therefore, if a record of translational seismic motion contains both body as well as surface waves then, in order to accurately estimate rotational motions, we must have the capability to separate surface from body waves so as to accurately estimate rotational motions from each set of waves. It should be mentioned that one of the earliest works to consider the potential simultaneous presence of both body and surface waves on recorded motion, and the necessity to treat them separately was Castellani and Boffi [4,5]. Meza-Fajardo et al. [14] have proposed an effective procedure (referred to as 'Normalized Inner Product' procedure or 'NIP' for short) to identify and extract surface waves from a given translational record of ground motion. The procedure is based on the S-Transform [16] and can be used successfully to identify (and subsequently extract) Rayleigh waves (separately retrograde and prograde) as well as Love waves. Once the surface waves have been extracted, they can be processed appropriately to provide estimates of rotational motions (i.e., rocking or torsion).

In the present work we apply the 'NIP' procedure to identify and extract surface waves and, exploiting the absolutely referenced phase information of the S-Transform, we employ it in cross-spectrum analysis in a local manner, as originally proposed by Stockwell [17]. Specifically, by considering two 'sufficiently' close recording stations ('sufficiency' in proximity of the stations is judged by comparing the wavelengths of the signal to be analyzed with the distance of the two stations projected on the direction of propagation of the signal), the cross-correlation of the 'voices' of the S-Transforms at the two stations, for a selected frequency f, can provide the phase difference at that particular frequency f. This phase difference, combined with the distance of the stations, can provide the phase velocity of the signal at frequency f. Thus, after identifying and extracting the surface waves of a recorded motion, we can apply Newmark's [15] approach to estimate rotational motions using the estimates of phase velocities described above.

We apply the proposed angular displacement estimation procedure for two well recorded data sets: (1) the strong motion data generated by an aftershock of the 1999 Chi-Chi, Taiwan earthquake and recorded over the Western Coastal Plain (WCP) of Taiwan, and (2) the strong motion data generated by the 2010 Darfield, New Zealand earthquake and recorded over the Canterbury basin. The former data set is dominated by basin-induced Rayleigh waves while the latter contains primarily Love waves.

2. Time–frequency extraction of love waves using the NIP

In this section we present a procedure to compute the direction of polarization (and consequently the direction of propagation) of Love waves, which does not require the previous computation of the direction of Rayleigh waves. The advantage of this method is that the calculated angle of polarization is not affected by the assumption regarding the type of Rayleigh wave motion which is present in the signal, that is, whether the Rayleigh wave is prograde or retrograde. Furthermore, because the computation of the angle of polarization does not involve the vertical component, the proposed procedure is free of errors that are introduced when the vertical component is of such low amplitude than may be buried in noise.

As in Meza-Fajardo et al. [14] we perform our analysis using time–frequency representations of the components of the signal. We use the Stockwell Transform to map a time-domain component $h(t)$ in the time–frequency domain (τ,f), which is defined in the following form:

$$S(\tau,f)=\int_{-\infty}^{\infty} h(t)\frac{|f|}{\sqrt{2\pi}}\exp\left[-\frac{(\tau-t)^2f^2}{2}\right]\exp\left[-2\pi i f t\right]dt \tag{1}$$

Let us note that since the Stockwell Transform representation of a real function is a complex valued function, with amplitude $A(\tau,f)$ and phase $\Phi(\tau,f)$, it can be expressed as:

$$S(\tau,f)=\mathscr{R}e\left[S(\tau,f)\right]+i.\mathscr{I}m\left[S(\tau,f)\right]=A(\tau,f)e^{i\Phi(\tau,f)} \tag{2}$$

In Meza-Fajardo et al. [14] we used the Normalized Inner Product of the vertical and one horizontal component as criterion to identify and extract Rayleigh waves. The NIP can be considered as the time–frequency counterpart of the correlation of signals in the time domain. Thus it can be used to identify and isolate those areas in the (τ,f) domain where the signal components are most (or least) correlated. In the present work we again use the NIP, to extract Love waves, considering only horizontal components. The NIP of two time–frequency components $S_l(\tau,f)$ and $S_m(\tau,f)$ can be

defined as follows:

$$\mathrm{NIP}\left[S_l(\tau,f),S_m(\tau,f)\right] = \cos\left[\Phi_l(\tau,f)-\Phi_m(\tau,f)\right] = \frac{\mathscr{R}e\left[S_l(\tau,f)\right]\mathscr{R}e\left[S_m(\tau,f)\right]+\mathscr{I}m\left[S_l(\tau,f)\right]\mathscr{I}m\left[S_m(\tau,f)\right]}{A_l(\tau,f)A_m(\tau,f)} \tag{3}$$

When the Inner Product (IP) is not normalized it can be evaluated as follows:

$$\mathrm{IP}\left[S_l(\tau,f),S_m(\tau,f)\right] = A_l(\tau,f)A_m(\tau,f)\cos\left[\Phi_l(\tau,f)-\Phi_m(\tau,f)\right] \tag{4}$$

Note that if the amplitudes of the time–frequency components are different from zero, then, $\mathrm{NIP}\left[S_l(\tau,f),S_m(\tau,f)\right]=0$ can be simplified to $\mathrm{IP}\left[S_l(\tau,f),S_m(\tau,f)\right]=0$.

Love waves are known for being linearly polarized in the horizontal plane. This implies that, if the component of the signal containing the Love wave in the time domain is denoted by $x_{POL}(t)$, and the component normal to it by $x_{NRM}(t)$, the correlation between $x_{POL}(t)$ and $x_{NRM}(t)$ should be ideally zero (or, practically, close to zero). Furthermore, the correlation between the component $x_{POL}(t)$ and the vertical component $x_V(t)$ should be close to zero as well. Since correlation in the time domain is equivalent to the Normalized Inner Product (NIP) in the time–frequency domain, these two correlations can be expressed in the (τ,f) domain as follows:

$$\mathrm{NIP}\left[S_{POL}(\tau,f),S_{NRM}(\tau,f)\right]=0, \qquad \mathrm{NIP}\left[S_{POL}(\tau,f),S_V(\tau,f)\right]=0 \tag{5}$$

where $S_{POL}(\tau,f), S_{NRM}(\tau,f)$, and $S_V(\tau,f)$ are the time–frequency counterparts of $x_{POL}(t)$, $x_{NRM}(t)$, and $x_V(t)$, respectively. Now, in most cases the analyst does not know the direction of the component $x_{POL}(t)$, and the horizontal components of the signals are usually provided in North–East components or in directions related to the positioning of the recording instrument. That is why here we make use of the NIP criterion to estimate the direction of polarization of Love waves, that is, the direction of the $x_{POL}(t)$ component. However, let us note that dispersed waves (such as surface waves) appear in a time history as narrow-band wave packets, and several wave packets (or wave trains) polarized in different directions can be present in the signal at different time intervals. Therefore, in this derivation we assume the signal contains only one wave train, such that the 'average' direction of polarization of the wave train will not change with time. If the signal happens to contain wave trains at different time intervals, each interval needs to be addressed separately. This assumption allows us to exploit the linearity of the Stockwell Transform, to relate the known and unknown horizontal time–frequency components of the signal by a simple coordinate transformation as follows:

$$\begin{pmatrix} S_{POL}(\tau,f) \\ S_{NRM}(\tau,f) \end{pmatrix} = \begin{bmatrix} \cos\theta & \sin\theta \\ -\sin\theta & \cos\theta \end{bmatrix} \begin{pmatrix} S_N(\tau,f) \\ S_E(\tau,f) \end{pmatrix} \tag{6}$$

where $S_N(\tau,f)$ and $S_E(\tau,f)$ denote the Stockwell Transform of the North and East components of the signal, respectively. Here the angle θ represents the azimuth (angle measured clockwise from the North) giving the direction of particle motion polarization; the direction of the normal component is obtained by adding clockwise 90° to the angle θ. To find such angle, we will make use of the Inner Product criterion as we explain below.

In our previous work [14], in order to find the direction of polarization of a Rayleigh wave, we made use of the relation $\mathrm{IP}\left[S_{NRM}(\tau,f),S_{\overline{V}}(\tau,f)\right]=0$, where $S_{\overline{V}}(\tau,f)$ is the vertical component with a $\pi/2$ phase shift. We have now found that such relation can be problematic in finding the direction of polarization of surface waves if the vertical component is so small that its amplitude is comparable to that of the signal's noise. This can be the case if the signal is composed mainly of Love waves, for which we expect very small or zero vertical component. Therefore, in order to find the direction of polarization of a Love wave, we make use of the more convenient relation $\mathrm{IP}\left[S_{POL}(\tau,f),S_{NRM}(\tau,f)\right]=0$, and substitute the transformation given in (6):

$$\mathrm{IP}\left[\left\{S_N(\tau,f)\cos\theta+S_E(\tau,f)\sin\theta\right\},\left\{-S_N(\tau,f)\sin\theta+S_E(\tau,f)\cos\theta\right\}\right]=0 \tag{7}$$

Using the properties of the Inner Product, we obtain the following trigonometric equation, since we are seeking to determine the angle θ:

$$\left\{\mathrm{IP}\left[S_E(\tau,f),S_E(\tau,f)\right]-\mathrm{IP}\left[S_N(\tau,f),S_N(\tau,f)\right]\right\}\cos\theta\,\sin\theta+\mathrm{IP}\left[S_N(\tau,f),S_E(\tau,f)\right]\left(\cos^2\theta-\sin^2\theta\right)=0 \tag{8}$$

To solve Eq. (8), we apply the trigonometric identities of the double angle:

$$\left\{\mathrm{IP}\left[S_E(\tau,f),S_E(\tau,f)\right]-\mathrm{IP}\left[S_N(\tau,f),S_N(\tau,f)\right]\right\}\frac{\sin 2\theta}{2}+\mathrm{IP}\left[S_N(\tau,f),S_E(\tau,f)\right]\cos 2\theta=0 \tag{9}$$

Assuming $\theta\neq\frac{\pi}{4}+n\frac{\pi}{2}$, $n=0,1,2,3\ldots$, we can divide by $\cos 2\theta$ and solve for $\tan 2\theta$:

$$\tan 2\theta=\frac{2\cdot\mathrm{IP}\left[S_N(\tau,f),S_E(\tau,f)\right]}{\mathrm{IP}\left[S_N(\tau,f),S_N(\tau,f)\right]-\mathrm{IP}\left[S_E(\tau,f),S_E(\tau,f)\right]} \tag{10}$$

Now, because $\mathrm{IP}\left[S_l(\tau,f),S_l(\tau,f)\right]=A_l^2(\tau,f)$, Eq. (10) can be expressed as:

$$\theta_r=\frac{1}{2}\tan^{-1}\left\{2\frac{\mathrm{IP}\left[S_N(\tau,f),S_E(\tau,f)\right]}{A_N^2(\tau,f)-A_E^2(\tau,f)}\right\} \tag{11}$$

In the latter equation we make use of the subscript 'r' in the angle θ, because Eq. (11) provides only the 'reference' angle, which varies in the range $(-\pi/4,\pi/4)$. The quadrant where the angle θ is located should be determined by examining the signs of the function $\tan 2\theta$. We do this by noting the following relations:

$$\begin{aligned}\mathrm{sign}(\sin 2\theta)&=\mathrm{sign}(2\sin\theta\cos\theta)\\ \mathrm{sign}(\cos 2\theta)&=\mathrm{sign}(2\cos^2\theta-1)\end{aligned} \tag{12}$$

and making use of Table 1 which provides the signs of the trigonometric functions: $\sin\theta$, $\cos\theta$, $\sin(2\theta)$, $\cos(2\theta)$, and $\tan(2\theta)$, as θ varies in the range $(0,2\pi)$. Thus, we can use the

Table 1
Table of signs of trigonometric functions of interest.

Range of θ	sign($\sin\theta$)	sign($\cos\theta$)	sign($\sin 2\theta$)	sign($\cos 2\theta$)	sign($\tan 2\theta$)
$0\le\theta<\pi/4$	+	+	+	+	+
$\pi/4<\theta\le\pi/2$	+	+	+	−	−
$\pi/2\le\theta<3\pi/4$	+	−	−	−	+
$3\pi/4<\theta\le\pi$	+	−	−	+	−
$\pi\le\theta<5\pi/4$	−	−	+	+	+
$5\pi/4<\theta\le3\pi/2$	−	−	+	−	−
$3\pi/2\le\theta<7\pi/4$	−	+	−	−	+
$7\pi/4<\theta\le2\pi$	−	+	−	+	−

following expression to determine θ in the correct quadrant:

$$\theta = \theta_r + \pi/4[1 - \text{sign}(\cos 2\theta)]\,\text{sign}(\sin 2\theta) \quad (13)$$

However, as we observe in Table 1, there are two possible ranges of θ for each combination of signs of $\sin 2\theta$ and $\cos 2\theta$. For example, if both $\sin 2\theta$ and $\cos 2\theta$ are positive, the angle can be in the range $0 \le \theta < \pi/4$, or in the range $\pi \le \theta < 5\pi/4$. We note that for all cases, there is a difference of π between the two possible ranges. Thus, in order to choose the correct range of the angle θ, we need to consider not only the signs of the functions $\sin 2\theta$ and $\cos 2\theta$, but also whether the function $\sin\theta$ is positive or negative in the quadrant of θ. If $\sin\theta$ is positive, we will then know that the range for the angle of the example is $0 \le \theta < \pi/4$. Thus, the analyst has to decide the sign of $\sin\theta$ to assign the correct quadrant of θ. This choice can be linked to the sense of propagation of the phase/signal under consideration. If θ gives the direction of polarization of the Love wave, its direction of propagation will be given by θ_{PRO} which is measured 90° clockwise from θ. Now the analyst, based on what the data indicates, can assess whether the direction of propagation of the Love wave is Eastwards ($\sin\theta_{PRO} > 0$) or Westwards ($\sin\theta_{PRO} < 0$). Therefore, to introduce the choice of the sense of propagation so we can eliminate the ambiguity, we propose the following expression:

$$\theta_{POL} = \theta + \pi/2\{\text{sign}[\sin(\theta + \pi/2)] - \text{sign}[\sin\theta_{PRO}]\} \quad (14)$$

where θ_{POL} is the angle giving the final (corrected) direction of polarization of the Love wave. This equation will simply add an angle π to the angle θ if sign($\sin\theta_{PRO}$) (chosen by the analyst) is opposite to the sign of $\sin(\theta + \pi/2)$ [θ computed with Eq. (13)]. If the signs are equal, the added angle is zero because there is no need of correction.

Now, it is important to remark that the azimuth θ_{POL} we compute with Eq. (14) will not be a single number, but another function in the time–frequency domain. With the function $\theta_{POL}(\tau, f)$, the transformation of Eq. (6) can then be used to compute the time–frequency components $S_{POL}(\tau, f)$ and $S_{NRM}(\tau, f)$. The Love wave is supposed to be found in the $S_{POL}(\tau, f)$ component, and thus its time-domain waveform $x_{POL}(t)$ can be obtained by simply applying the inverse Stockwell Transform to $S_{POL}(\tau, f)$. However, let us recall that the initial assumption to derive Eq. (14) to compute the angle θ_{POL} is that the Inner Product between the two horizontal components of the wave, S_{POL} and S_{NRM}, is zero. Such condition is met by Love as well as Rayleigh waves. But Rayleigh waves are elliptically polarized in a vertical plane, therefore the horizontal component in the direction of polarization $x_{POL}(t)$ and the vertical component $x_V(t)$ are $\pi/2$ rad out of phase. If the vertical component is shifted $\pi/2$ rad (phase delay or phase advance, depending whether the particle motion is prograde or retrograde) the resulting vertical component will be in phase with (and thus highly correlated to) the $x_{POL}(t)$ component. We can discern then whether the wave in the $x_{POL}(t)$ component is a Rayleigh or a Love wave by computing the correlation coefficient in the time domain, given by:

$$C_{P\bar{v}} = \frac{\sum_1^n x_{POL}(i)\overline{x_v}(i)}{\sqrt{\left[\sum_1^n x_{POL}(i)x_{POL}(i)\right]\left[\sum_1^n \overline{x_v}(i)\overline{x_v}(i)\right]}} \quad (15)$$

If this coefficient is close to 0, then we can conclude that the wave in the $x_{POL}(t)$ component is a Love wave. If, on the other hand, the coefficient $C_{P\bar{v}}$ is far from zero, then we should investigate whether a Rayleigh wave is present in the signal.

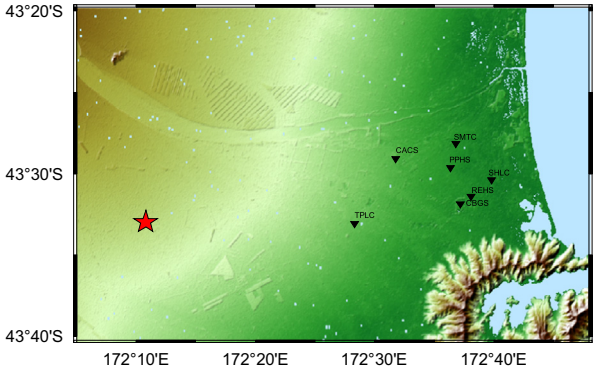

Fig. 1. Location of stations on the Canterbury basin and location of epicenter (indicated by the star) of the 2010 Darfield earthquake in New Zealand.

3. Extraction of Love waves from recordings of the 2010 Darfield earthquake

In this section we illustrate how to compute the direction of polarization of Love waves from real seismograms. We use the three-component seismograms recorded in the Canterbury basin during the 2010 Darfield earthquake. We chose this event because the fault is buried under a thick (~700 m) sedimentary basin, and the earthquake is a large (M_w=7.1) strike slip event. Under such conditions significant amounts of seismic energy are expected to

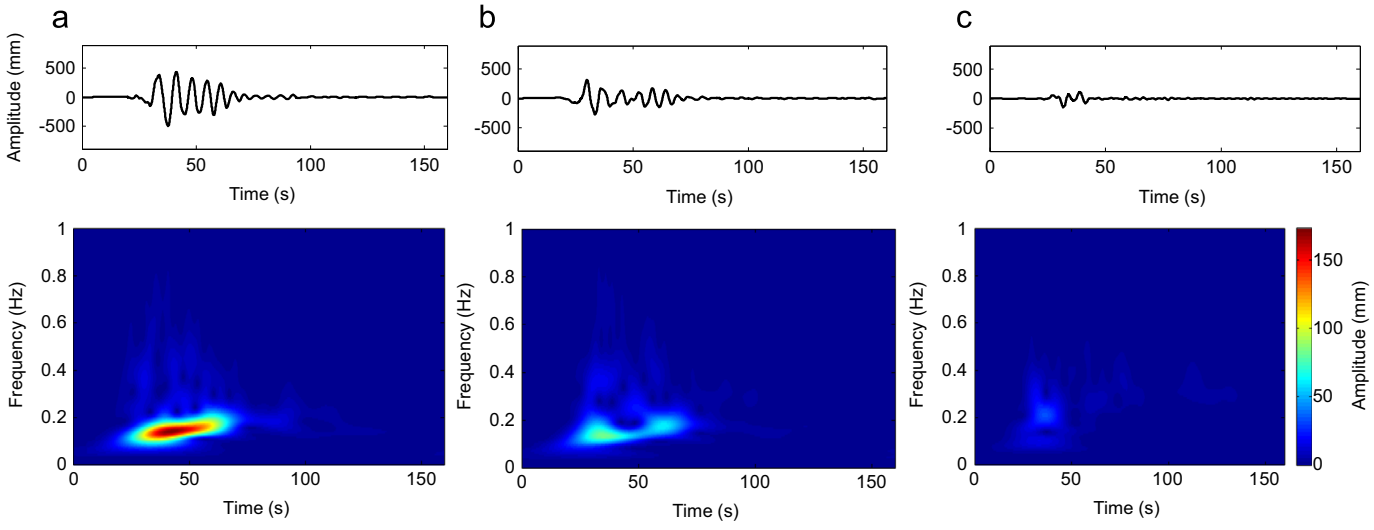

Fig. 2. Seismograms at station CACS. (a) North component (b) East component and (c) vertical component.

propagate in the form of Love waves over the Canterbury basin (e.g., [1]). The locations of the epicenter and the stations considered in this study are shown in Fig. 1. We start by analyzing the recordings at station CACS. The time domain and time–frequency domain North, East and Vertical components are shown in Fig. 2. We can observe that most of the energy is contained in the North component, and that, as expected, the vertical component is rather weak. We then use Eqs. (13) and (14) to compute the time–frequency parameter θ_{POL} shown in Fig. 3, where we have chosen the sense of propagation of the waves to be Eastward. In Fig. 3 we can observe that the direction of polarization between 0 and 70 s, for the waves below 0.2 Hz is very close to the North direction, a result that is compatible with Love waves propagating from West to East. However the exact numerical value of the direction of polarization is not given in Fig. 3 yet. Before computing the angle giving that direction, we need to extract the waveforms of the Love waves. Now we use the obtained angle θ_{POL} to compute the time–frequency parameters S_{POL} and S_{NRM} using Eq. (6), obtaining the results shown in Fig. 4. We can observe that the energy is mainly located in the component S_{POL}, where we expect to find the Love wave. At this stage it is important to remark that the initial assumption to derive the angle θ_{POL} is that the inner product between the two horizontal components of the wave S_{POL} and S_{NRM} is zero. Such condition is met by Love as well as Rayleigh waves. The type of wave present in the signal can then be identified by how the time-domain components $x_{POL}(t)$ and $x_v(t)$ are correlated. Therefore, we apply the inverse Stockwell Transform to the time–frequency components S_{POL} and S_{NRM} to obtain the time-domain horizontal waveforms $x_{POL}(t)$ and $x_{NRM}(t)$, shown in Fig. 5. It can be observed that also in the time domain there is little energy in the component $x_{NRM}(t)$. Now, the correlation coefficient $C_{P\bar{v}}$ given in (15) will indicate the type of surface wave we are extracting:

$$C_{P\bar{v}} = 0.0588 \tag{16}$$

With such low correlation coefficient we can be certain there are no Rayleigh waves in the signal. If, on the other hand, the coefficient $C_{P\bar{v}}$ is far from zero, we could then apply a filter that will exclude both prograde and/or retrograde Rayleigh waves, using the condition proposed in Meza-Fajardo et al. [14]:

$$\mathrm{NIP}\left[S_{POL}(\tau,f), \bar{S}_V(\tau,f)\right] \approx 1 \tag{17}$$

where $\bar{S}_V$ is shifted vertical component in the time–frequency domain.

Now that the Love wave has been extracted, the time-domain component $x_{POL}(t)$ is used to compute the azimuth of its angle of polarization φ, with the following expression:

$$\tan\varphi_r = \frac{S_{EP}}{S_{NP}} = \frac{\sum_1^n x_E(i)x_{POL}(i)}{\sum_1^n x_N(i)x_{POL}(i)}$$

$$\varphi = \varphi_r + \pi[1-\mathrm{sign}(S_{EP})] + \pi[1-\mathrm{sign}(S_{NP})]\mathrm{sign}(S_{EP})/2 \tag{18}$$

where $x_N(t)$, $x_E(t)$, are the time-domain North and East components of the signal, respectively. For station CACS the obtained angle of polarization is 337.1833°. This angle can be further used to confirm if the waveform we extracted in the time–frequency domain is correct, by rotating the original North and East time-domain components with the following transformation:

$$\begin{pmatrix} x_{POL}(t) \\ x_{NRM}(t) \end{pmatrix} = \begin{bmatrix} \cos\varphi & \sin\varphi \\ -\sin\varphi & \cos\varphi \end{bmatrix} \begin{pmatrix} x_N(t) \\ x_E(t) \end{pmatrix} \tag{19}$$

The results are shown in Fig. 6. When comparing with Fig. 5, we can affirm the waveforms $x_{POL}(t)$, obtained by rotation in the time and the time–frequency domains, are practically the same. For the normal component $x_{NRM}(t)$ the results are different, because the low intensity of the waves in its direction makes it more susceptible to the errors introduced by the arithmetic operations associated with the transformation of the signal to the time–frequency domain, its inversion, and its rotation. However, we are not interested in the waves of the $x_{NRM}(t)$ component, the surface waves we seek to extract are in the direction of the $x_{POL}(t)$ component. The advantage of computing the components $[x_{POL}(t), x_{NRM}(t)]$ by rotation in the time domain is their precise physical meaning: wave components in two orthogonal directions given by the azimuth φ. However this computation can be done only after we have computed the azimuth φ by rotating and extracting the waves in the time–frequency domain.

Finally, we confirm one last time the wave in the component $x_{POL}(t)$ is a Love wave (as shown in Fig. 6, by computing the

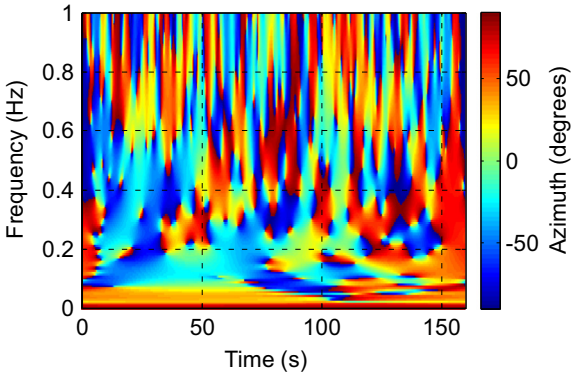

Fig. 3. Time–frequency direction of polarization at station CACS.

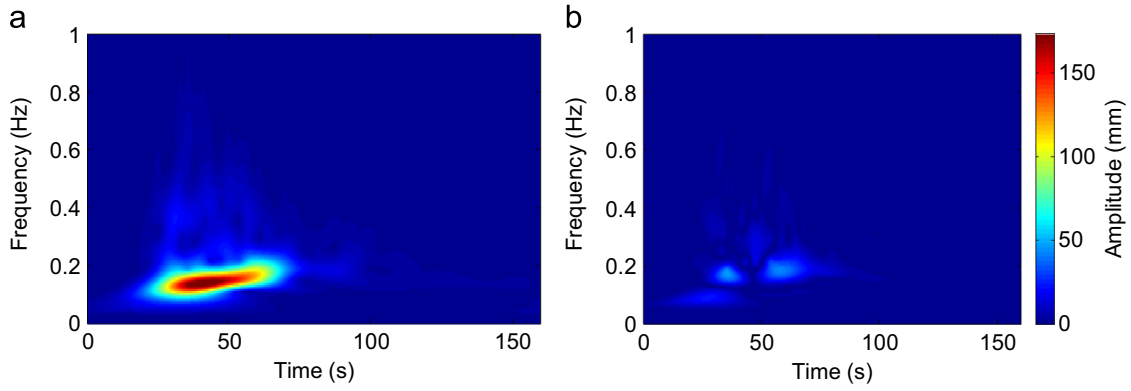

Fig. 4. Time frequency horizontal components at station CACS. (a) Amplitude of S_{POL} component, and (b) amplitude of S_{NRM} component.

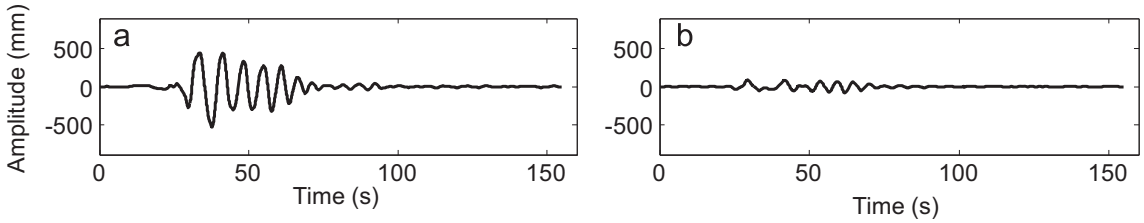

Fig. 5. Inverted components at station CACS. (a) x_{POL} component, and (b) x_{NRM} component.

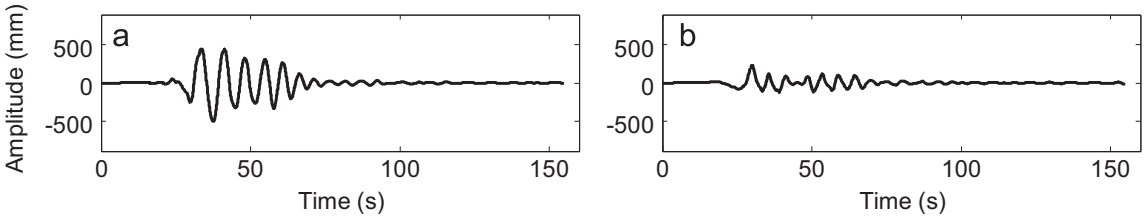

Fig. 6. Horizontal components at station CACS corresponding to an azimuth of 337.1833°. (a) x_{POL} component, and (b) x_{NRM} component x_{NRM}.

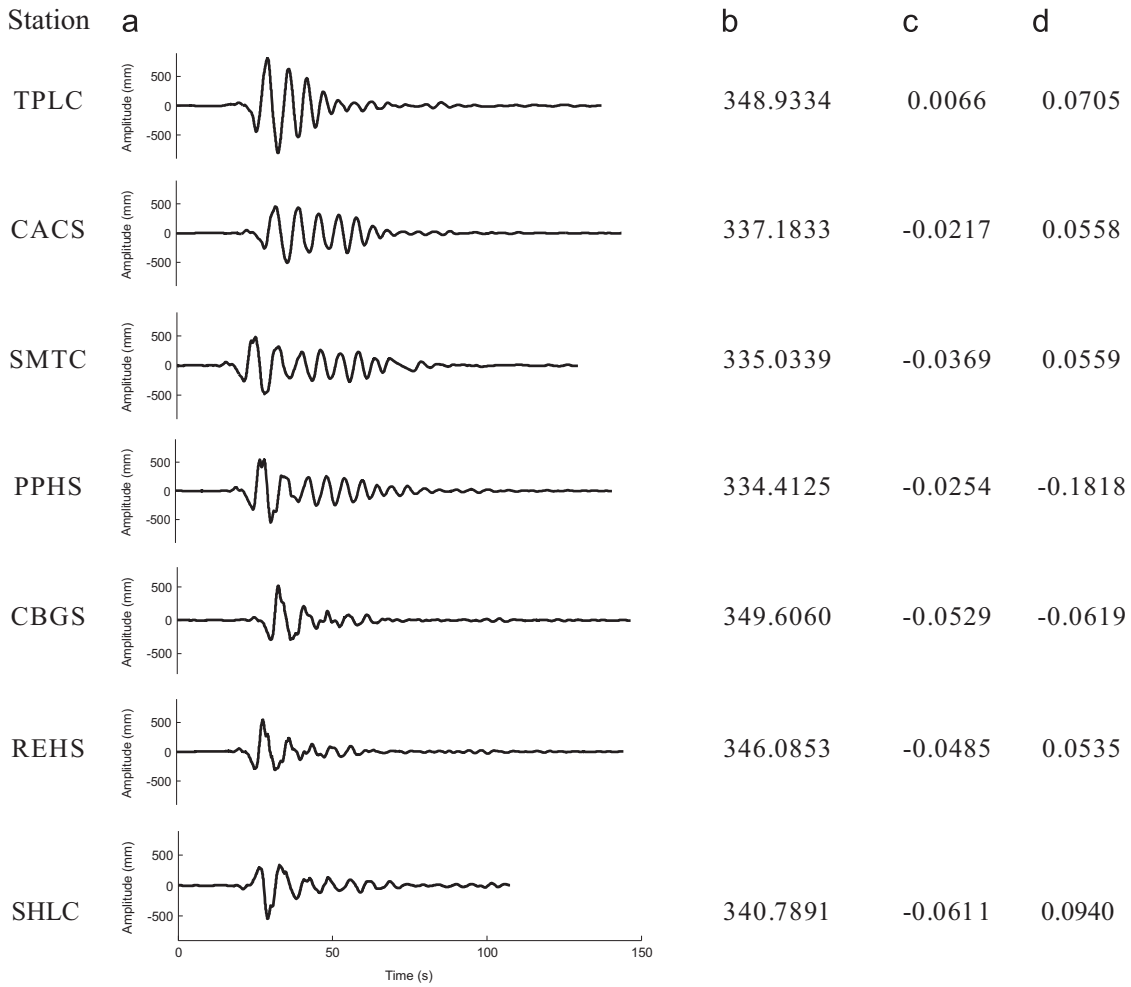

Fig. 7. Love waves extracted from recordings at different stations in the Canterbury basin during the 2010 Darfield earthquake, New Zealand. (a) x_{POL} component, (b) azimuth direction of polarization (deg), (c) correlation coefficient between x_{POL} and components, C_{PN}, and (d) correlation coefficient between x_{POL} and phase advanced vertical components, $C_{P\tilde{V}}$.

correlation coefficients between the components, $x_{POL}(t)$ and $x_{NRM}(t)$:

$$C_{PN} = \frac{\sum_1^n x_{POL}(i)x_{NRM}(i)}{\sqrt{\left[\sum_1^n x_{POL}(i)x_{POL}(i)\right]\left[\sum_1^n x_{NRM}(i)x_{NRM}(i)\right]}} = -0.0217 \qquad (20)$$

which is a very low value, as expected. In Fig. 7 we present the component $x_{POL}(t)$ containing Love waves at other selected stations on the Canterbury basin computed using the same procedure presented in this section. Because of the low correlation coefficients we can affirm that they are Love waves.

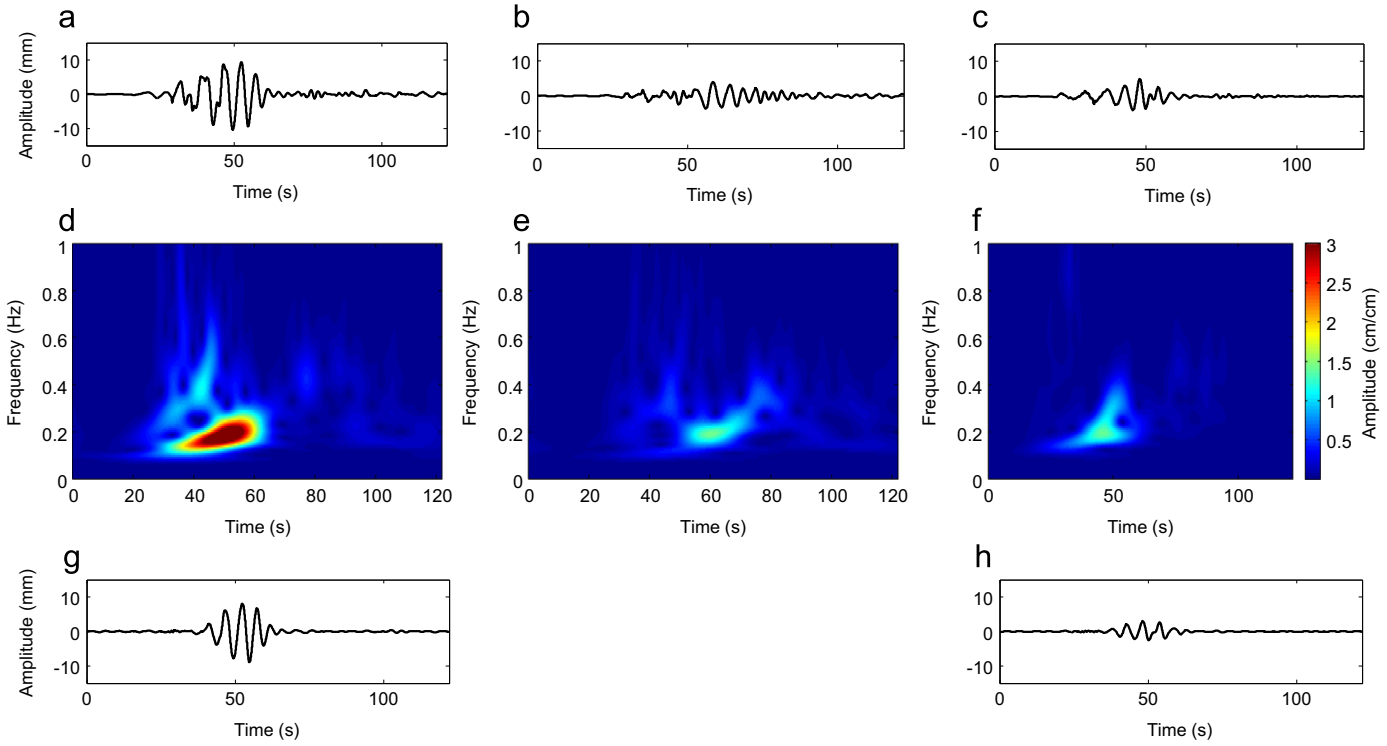

Fig. 8. Seismograms at station TCU118. (a) Unfiltered x_{POL} component with azimuth of 304.776° (b) unfiltered component (c) unfiltered vertical Component (d) unfiltered S_{POL} component (e) unfiltered S_{NRM} component (f) unfiltered S_V component (g) x_{POL} component of extracted Rayleigh wave and (h) Vertical component of x_{NRM} extracted Rayleigh wave.

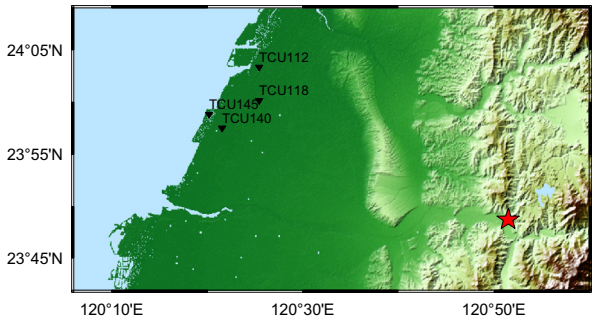

Fig. 9. Location of stations on the Western Coastal Plain and location of epicenter (indicated by the star) of the 1999 Chi-Chi earthquake in Taiwan.

4. Rayleigh and Love waves from a recording of the 1999 Chi-Chi earthquake

A technique similar to what we present in the previous section was used in Meza-Fajardo et al. [14] to extract Rayleigh waves. The main difference between the two techniques is whether we use or not the vertical component of the recording to compute the angle of polarization/propagation given by (13). Besides, because for Rayleigh waves the direction of polarization coincides with the direction of propagation, Eq. (14) changes to:

$$\theta_{POL} = \theta + \pi/2\{\text{sign}[\sin\theta] - \text{sign}[\sin\theta_{PRO}]\} \tag{21}$$

where $\text{sign}[\sin\theta_{PRO}]$ is positive if the chosen sense of wave propagation is Eastwards, or negative if the sense of propagation is Westward. To show that with the two procedures we obtain similar results, here we consider the seismogram of the 1999 Chi-Chi event recorded at station TCU118 on the Western Coastal Plain in Taiwan. The original displacement histories are shown in Fig. 8 (a)–(c), where the two horizontal components have been rotated with an azimuth of 304.776°. We explain below how this azimuth is computed. The location of the station and the earthquake epicenter are shown in Fig. 9. In Meza-Fajardo et al. [14] we extracted both types of waves, first Rayleigh (retrograde) waves and then Love waves, from the recording at this station. Here, with the new procedure, we try first to extract the Love waves. Using Eqs. (12 and 13) we compute the S_{POL}, components in the time–frequency domain, which are shown in Fig. 8(d) and (e). We can observe in Fig. 8(d) and (e) that even though most of the energy is located in the S_{POL} component, there is an important wave train in the S_{NRM}. component as well. Now, we obtain the time domain component $x_{POL}(t)$ from inverting S_{POL}, and investigate what its correlation with the vertical component is. The value we obtain for the correlation coefficient $C_{P\bar{v}}$ given in Eq. (15) is:

$$C_{P\bar{v}} = -0.4095 \tag{22}$$

With this high value we can confirm that in the signal there are waves with important vertical component, possibly Rayleigh waves. Therefore, with the new procedure, we proceed extracting the Rayleigh waves from the displacement histories, by applying a time–frequency filter to both the S_{POL} and S_V components, as follows:

$$F(x) = \begin{cases} 0 & x < 0.7 \\ \frac{1}{2}\cos\left[\frac{\pi(x-0.8)}{0.1}\right] + \frac{1}{2} & 0.7 < x < 0.8 \\ 1 & 0.8 < x \end{cases} \tag{23}$$

where $x = \text{NIP}\left[S_{POL}(\tau,f), \bar{S}_V(\tau,f)\right]$. , and $\bar{S}_V$ is phase advanced vertical component in the time–frequency domain. In theory the $\text{NIP}\left[S_{POL}(\tau,f), \bar{S}_V(\tau,f)\right]$ for a Rayleigh wave is 1, but in a real signal we expect this value to be close to 1 (thus the 0.8 value). Then we leave a margin of 0.1 so that the filter can smoothly go from 0 to 1 (with a cosine taper) in order to minimize errors due to the filtering process. Filter (23) will then exclude the regions of the

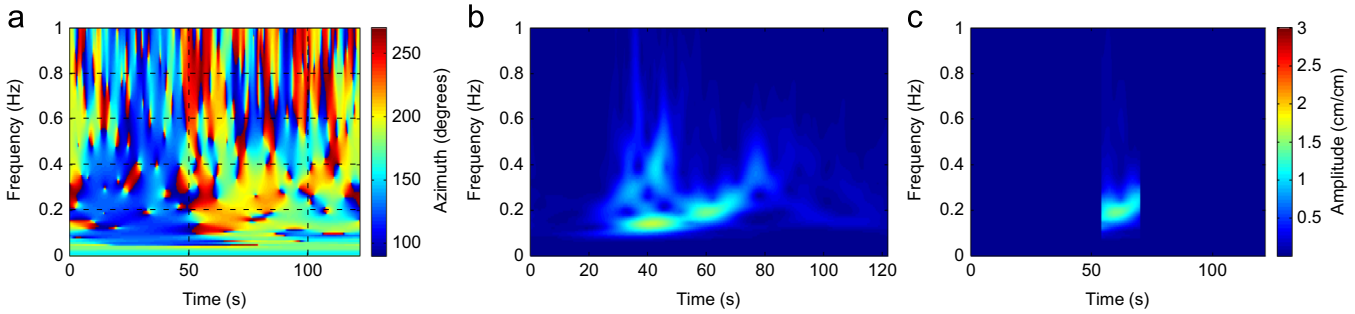

Fig. 10. Time–frequency components at station TCU118 after Rayleigh waves have been excluded. (a) Angle of polarization (b) amplitude of S_{POL} component and (c) amplitude of filtered S_{POL} component.

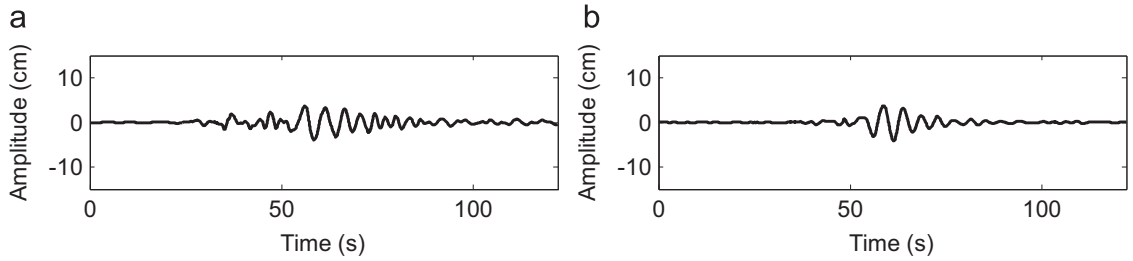

Fig. 11. Extracted Love waves at station TCU118. (a) waves extracted with the proposed procedure, (b) waves extracted as in Meza-Fajardo et al. [14].

time–frequency domain where the correlation between the horizontal and the shifted vertical component are less than 0.7. After the time–frequency components S_{POL} and S_V are filtered, they are inverted to obtain the time-domain extracted Rayleigh waves shown in Fig. 8(g) and (h). The waveforms we obtain are similar to those reported in Meza-Fajardo et al. [14] (compare Fig. 8(g) and (h) of the present work with Fig. 23(a) and (b) of Meza et al. 2015). The azimuth for the direction of propagation we compute with Eq. (18) is 304.776° whereas in Meza-Fajardo et al. [14] the computed angle was 304.51°. With an azimuth of 304.776° the correlation coefficient C_{PN} between the two horizontal components x_{POL} and x_{NRM} is 0.0336, and the correlation coefficient $C_{P\bar{v}}$ between the shifted vertical component and the component x_{POL} is 0.8494. Thus, the extracted waves have the polarization characteristics of Rayleigh waves. Now, to find the Love waves that are also present in the seismogram, we *exclude* the Rayleigh waves from the original signals applying the following filter $G(x)$ to the the S_{POL} and S_V components:

$$G(x) = 1 - F(x) \tag{24}$$

After inverting the filtered components back to the time domain, we rotate them to obtain the North–East components of the remaining waves. Now that the Rayleigh waves have been excluded, we start over the procedure of wave identification, this time in search for Love eaves. We use the S-Transforms of the new North and East components to compute the angle θ_{POL} for Love waves with Eqs. (13) and (14), with the results shown in Fig. 10(a). With this angle a new component S_{POL} is then obtained, illustrated in Fig. 10(b). We can observe that there are two wave trains in the S_{POL}. component, which can be considered as linearly polarized because they satisfy the relation NIP(S_{POL}, S_{NRM})=0 and the vertical component is weak. These two wavetrains are linearly polarized however in different directions as can be observed in Fig. 10(a), different angles can be read before and after 54 s. We claim that the Love wave is present after 54 s, because it is more dispersive and its direction of polarization is close to 200° (as indicated in Fig. 10(a)), almost perpendicular to the direction of propagation of the Rayleigh wave. The earlier wave on the other hand, is polarized in the direction of propagation, and it is probably a body wave or a reflection. Therefore, to isolate the Love wave, we filter out the wave train before 54 s and also the noise after 70 s, as shown in Fig. 10(c). After inverting the filtered S_{POL}. component of Fig. 10(c) we obtain an angle of polarization of 211.89° with Eq. (18). The direction of polarization for these waves, as estimated by Meza-Fajardo et al. [14], was 304.51 − 90 = 214.51°. We obtain a difference in the results of 214.51 − 211.89 = 2.62°. Thus, we can conclude that in this particular case, for which the vertical component has a high signal-to-noise ratio, the two discussed procedures (i.e., the one proposed in the present work and the one that wapresented and used by Meza et al. 2015) lead to similar results. Finally, the extracted Love waves are shown in Fig. 11. The waveform coincides with what was identified and extracted by Meza-Fajardo et al. [14], however the results obtained in the present work seem to have a more complete frequency content for the extracted Love wave.

5. Use of recorded translational motions to estimate rocking and torsion

In the previous section we presented and used a time–frequency technique to extract Rayleigh and Love waves from three-component seismograms. In this section, we continue exploiting the time–frequency resolution of translational ground motions to estimate rotational motions (i.e., rocking and torsion) from the extracted Rayleigh and Love waves.

Starting with elementary continuum mechanics (e.g., [13]) and considering a right-handed rectangular Cartesian coordinate system (x, y, z) (z being the vertical axis and x and y being the two horizontal axes), we denote by ψ the positive rotation about the y-axis (i.e., rocking) and by φ the positive rotation about the vertical z-axis (i.e., torsion) (in Malvern's notation, ψ and φ are denoted by ω_y and ω_z, respectively, and may be expressed in terms of the gradients of the displacement field).

Rocking: rocking motion is associated with Rayleigh waves or non-vertically incident plane *P*- or *SV*-waves (i.e., in-plane motions). Let a plane Rayleigh wave be moving in the (zx) plane. Then, rotation about the y-axis (i.e. rocking) at the free surface of

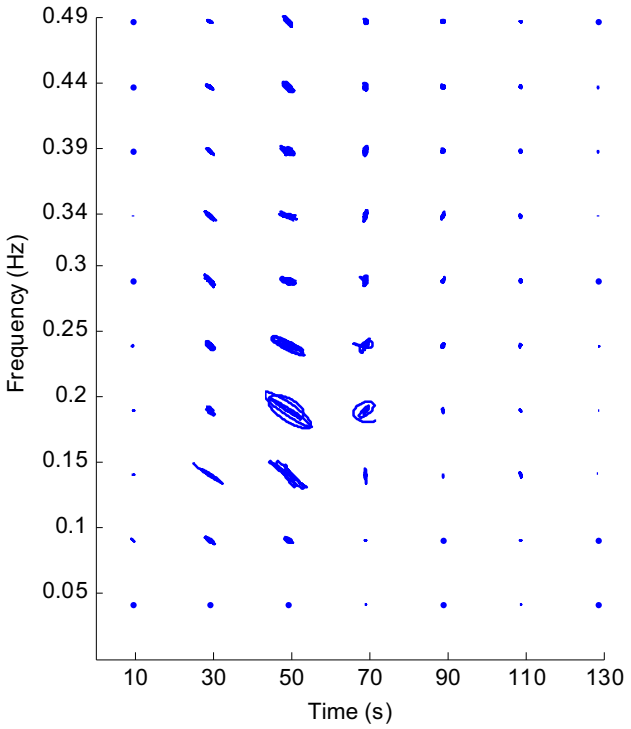

Fig. 12. North–East orbit spectrum for station TCU118.

the elastic half-space may be expressed in terms of the displacement gradients as follows:

$$\psi = \frac{1}{2} \backslash\backslash\backslash left\left(\frac{\partial u}{\partial z} - \frac{\partial w}{\partial x}\right)\Big|_{z=0} \tag{25}$$

The stress-free surface of the elastic half-space, at $z=0$, implies:

$$\tfrac{1}{2}\left(\tfrac{\partial u}{\partial z} + \tfrac{\partial w}{\partial x}\right)\Big|_{z=0} = 0 \tag{26}$$

Therefore, combining the above two equations, we obtain:

$$\psi = -\ \backslash\backslash\backslash left\left(\frac{\partial w}{\partial x}\right)\Big|_{z=0} \tag{27}$$

Torsion: torsional motion is induced by Love waves or by non-vertically incident plane SH-waves (i.e., out-of-plane motion). Let a plane Love wave be moving in the (zx) plane. Then, rotation about the z-axis (i.e. torsion) at the free surface of the elastic half-space is given by:

$$\varphi = -\frac{1}{2} \backslash\backslash\backslash left\left(\frac{\partial u}{\partial y} - \frac{\partial v}{\partial x}\right)\Big|_{z=0} \tag{28}$$

For a plain wave propagating in the (zx) plane, $\partial_y u = 0$. Introducing the latter condition in the above equation we obtain:

$$\varphi = \frac{1}{2} \backslash\backslash\backslash left\left(\frac{\partial v}{\partial x}\right)\Big|_{z=0} \tag{29}$$

Now, let $f\left(t - \frac{x}{c_{app}}\right)$ be the *waveform* of the displacement component v or w, propagating in the form a plane wave parallel to the x-axis towards the positive direction, with an apparent velocity c_{app} (i.e. the velocity with which the wave appears to propagate on the free surface).

Then, for rocking we have:

$$\psi = -\ \backslash\backslash\backslash left\left(\frac{\partial w}{\partial x}\right)\Big|_{z=0} = -\frac{\partial}{\partial x} f\left(t - \frac{x}{c_{app}}\right) = -\frac{df(\xi)}{d\xi} \cdot \left(-\frac{1}{c_{app}}\right) \tag{30}$$

Therefore:

$$\psi = \left(\frac{\dot{w}}{c_{app}}\right) \tag{31}$$

Similarly, for torsion we obtain:

$$\varphi = -\left(\frac{1}{2}\right)\left(\frac{\dot{v}}{c_{app}}\right) \tag{32}$$

Surface waves (Rayleigh or Love) propagating in a layered medium are dispersed, that is c_{app} is frequency dependent (i.e. $c_{app} = c_R(\omega)$ for Rayleigh waves and $c_{app} = c_L(\omega)$. for Love waves, where $c_R(\omega)$ and $c_L(\omega)$ are the frequency dependent phase velocities of Rayleigh and Love waves, respectively, for the particular layered medium). Consequently, the above expressions are strictly valid only for harmonic waves.

Consider the Fourier transform pairs, $v(t) \leftrightarrow \tilde{v}(\omega)$ d $w(t) \leftrightarrow \tilde{w}(\omega)$, of the displacements, as well as the Fourier transform pairs, $\psi(t) \leftrightarrow \tilde{\psi}(\omega)$ and $\varphi(t) \leftrightarrow \tilde{\varphi}(\omega)$, of the rotations. Then, the aforementioned results may be expressed exactly as follows:

$$\tilde{\psi}(\omega) = \left(\frac{i\omega}{c_R(\omega)}\right) \cdot \tilde{w}(\omega) \tag{33}$$

$$\tilde{\varphi}(\omega) = -\left(\frac{1}{2}\right)\left(\frac{i\omega}{c_L(\omega)}\right) \cdot \tilde{v}(\omega) \tag{34}$$

Fourier synthesis of the above harmonic components renders the time histories of rocking $\psi(t)$ and torsion $\varphi(t)$.

is straightforward to demonstrate (see Appendix) that the above expressions, which relate the Fourier components of rotations with the Fourier components of translational motions, apply also for the 'voices' of the S-Transforms of the corresponding quantities (definitions of the S-Transform and its 'voices' can be found in the Appendix). Specifically,

$$S_\psi(\tau, \omega) = \left(\frac{i\omega}{c_R(\omega)}\right) \cdot S_w(\tau, \omega) \tag{35}$$

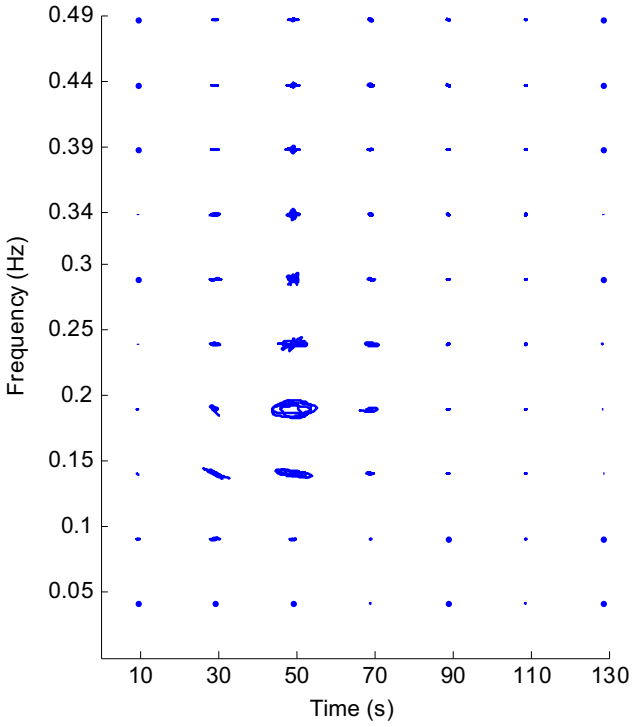

Fig. 13. Orbit spectrum in a vertical plane oriented in the direction of propagation for station TCU118.

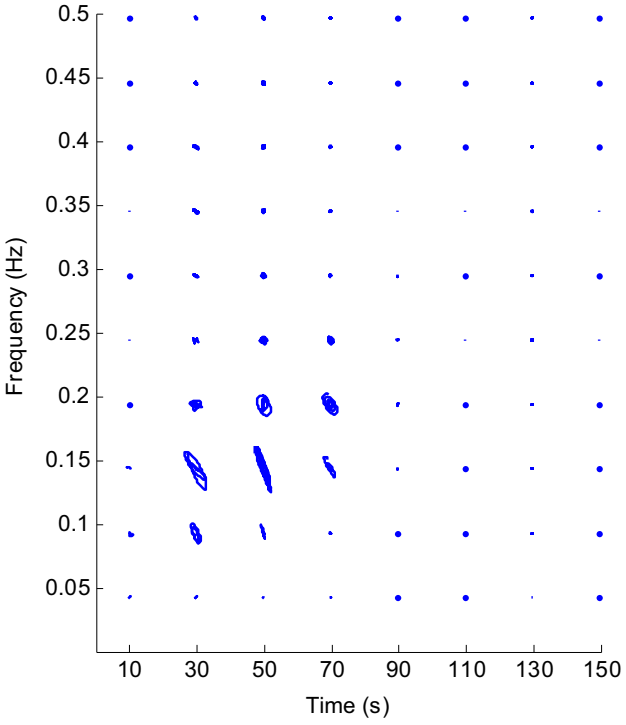

Fig. 14. North–East orbit spectrum for station CACS.

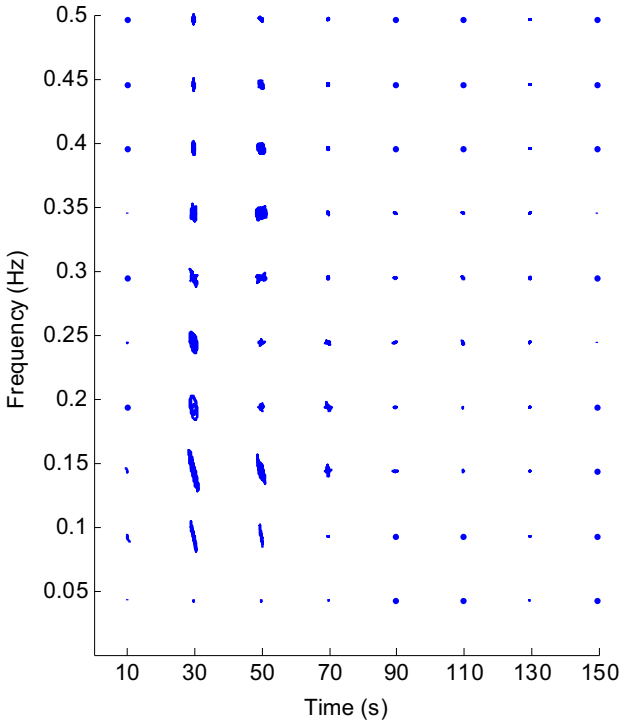

Fig. 16. North–East orbit spectrum for station CBGS.

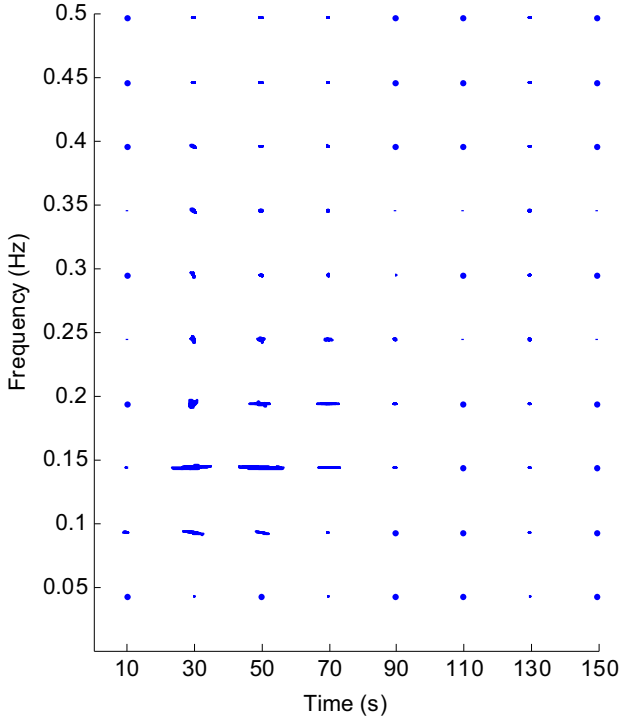

Fig. 15. Orbit spectrum in a vertical plane oriented in the direction of polarization for station CACS.

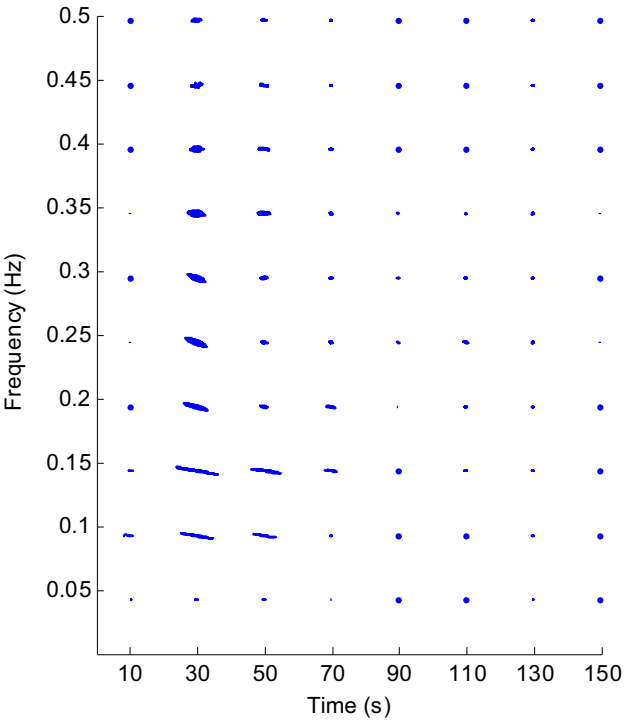

Fig. 17. Orbit spectrum in a vertical plane oriented in the direction of polarization for station CBGS.

$$S_{\varphi}(\tau,\omega) = -\left(\frac{1}{2}\right)\left(\frac{i\omega}{c_L(\omega)}\right)\cdot S_v(\tau,\omega) \tag{36}$$

Although both the Fourier components as well as the 'voices' of the S-Transform when inverted lead to the same result (i.e., the rotations $\psi(t)$ and $\varphi(t)$), use of the 'voices' is preferable because of the time-local information they provide, unlike the Fourier components [17]. This particular characteristic of the S-Transform makes possible the fruitful use of the '*Orbit Spectrum Analysis*' (e.g. [10]) which provides visual confirmation regarding the results of our identification and extraction technique for surface waves. Indeed, in Figs. 12 and 13 we display the results of Orbit Spectrum Analysis for the recording at station TCU118 of the 1803 aftershock during the 1999 Chi-Chi earthquake. The retrograde Rayleigh wave we had identified and extracted in our previous work (Meza et al. 2015) and considered in the present work too, had its energy

concentrated in the vicinity of 0.20 Hz, in a 20-s window centered at time 50 s, and its direction of propagation had an azimuth of 304.776° (for the time–frequency characteristics of this wave see Fig. 24(a) in Meza et al. 2015, and for its time history see Fig. 8 (g) and (h) of the present work). In Figs. 12 and 13 we display the polarization characteristics of this wave by plotting the orbits of selected 'voices' on the horizontal plane (Fig. 12) and on a vertical plane oriented in the radial direction (i.e., direction of propagation of the wave) (Fig. 13). From these figures it is clear that the wave is elliptically polarized on a vertical plane oriented in the radial direction, confirming the results of our identification analysis. Similarly, Figs. 14–17 display the polarization characteristics of the Love waves identified at stations CACS (Figs. 14 and 15) and CBGS (Figs. 16 and 17). The Love wave identified at station CACS has most of its energy in the vicinity of 0.15 Hz (Fig. 4) and over time window 20–60 s. From the results of the orbit analysis (Figs. 14 and 15) it is clear that the wave under consideration is linearly polarized in the direction transverse to the direction of propagation. Similar comments can be made also for the Love wave identified at station CBGS (Figs. 16 and 17).

6. Phase velocity from cross-spectrum analysis

Because of the *absolutely* referenced phase information of the Stockwell Transform, it can be employed in a cross-spectrum analysis to compute the phase velocities of the wave under consideration [17], as we explain in this section. Let us denote by $S_V^{(i)}(\tau,f)$ and $S_V^{(j)}(\tau,f)$ the Stockwell Transforms of the vertical components of the extracted Rayleigh waves, at two nearby stations i and j, respectively. The cross-spectrum of the Transforms is defined as follows:

$$\text{CrossST}(\tau,f) = S_V^{(i)}(\tau,f)\left\{S_V^{(j)}(\tau,f)\right\}^* \tag{37}$$

where with the symbol $\{\}^*$ we indicate the complex conjugate. Then, at each pair (τ,f), the cross-spectrum of the pair of stations under consideration, can be expressed as follows:

$$\text{CrossST}(\tau,f) = A_{CS}(\tau,f)\cdot e^{i\Phi_{CS}(\tau,f)} \tag{38}$$

where $A_{CS}(\tau,f)$ is the amplitude of the cross-spectrum at (τ,f), and $\Phi_{CS}(\tau,f) = \arg[\text{CrossST}(\tau,f)] = \Phi_i(\tau,f) - \Phi_j(\tau,f)$ is the phase of the cross-spectrum at (τ,f).

Now, for a selected frequency f_n, let τ_o be the time instant at which the amplitude of the cross-spectrum attains its maximum value A_o, i.e.

$$A_o = A_{CS}(\tau_o,f_n) = \max_{\tau} A_{CS}(\tau,f) \tag{39}$$

Now, the *phase lag* $\Delta\Phi(f_n)$ at the selected frequency f_n, between the voices $S_V^{(i)}(\tau,f_n)$ and $S_V^{(j)}(\tau,f_n)$ of the pair of stations under consideration, is defined as follows:

$$\Delta\Phi(f_n) = \Phi_{CS}(\tau_o,f_n) \tag{40}$$

If Δx is the distance (measured along the direction of propagation) of the two nearby stations, i and j, the phase velocity spectrum of the Rayleigh wave can be obtained with the simple expression:

$$c_R(f_n) = \frac{\Delta x}{\Delta\Phi(f_n)}(2\pi f_n) \tag{41}$$

The same procedure can be used to compute the phase velocity spectrum of Love waves, by considering the cross-spectrum of the Stockwell Transforms of the component containing them:

$$\text{CrossST}(\tau,f) = S_{POL}^{(i)}(\tau,f)\left\{S_{POL}^{(j)}(\tau,f)\right\}^* \tag{42}$$

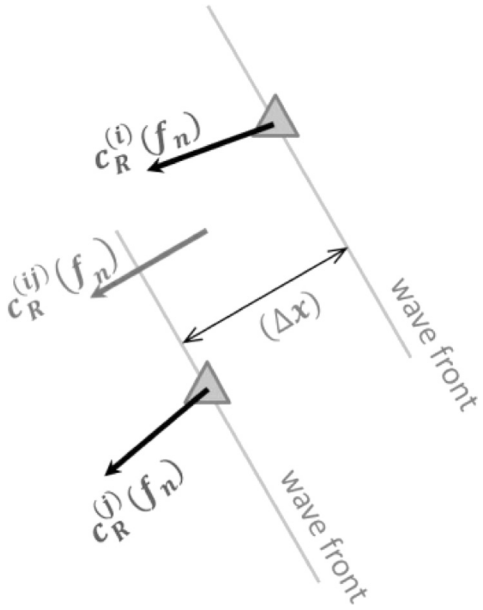

Fig. 18. Diagram of directions of propagation at two neighboring stations and the direction along which the distance Δx between them is computed.

Now ideally, if the wavefront of the wave under consideration, passing under the two neighboring stations, were plane, the direction of propagation of the wave as estimated at each station by the procedure we outlined earlier, would be the same for both stations. However, in practice, the numerical values of the direction of propagation of the wave estimated at the two stations would deviate from each other, normally by a small amount, as shown schematically in Fig. 18. In order to estimate an average direction of propagation we proceed as follows: Let θ_i and θ_j be the azimuthal angles of the direction of propagation estimated at stations i and j respectively. Then, the unit vectors $\mathbf{e}_{(i)}$ and $\mathbf{e}_{(j)}$ pointing towards the direction of propagation of the wave at the stations i and j, respectively, are given by the following expressions:

$$\mathbf{e}_{(i)} = \cos\left(\frac{\pi}{2}-\theta_i\right)\mathbf{i} + \sin\left(\frac{\pi}{2}-\theta_i\right)\mathbf{j} \quad \mathbf{e}_{(j)} = \cos\left(\frac{\pi}{2}-\theta_j\right)\mathbf{i} + \sin\left(\frac{\pi}{2}-\theta_j\right)\mathbf{j} \tag{43}$$

Then, the average direction of propagation, $\mathbf{e}_{(ij)}$, that we are seeking is given by:

$$\mathbf{e}_{(ij)} = \frac{1}{|\mathbf{e}_{(i)}+\mathbf{e}_{(j)}|}[\mathbf{e}_{(i)}+\mathbf{e}_{(j)}] \tag{44}$$

If (x_i,y_i) and (x_j,y_j). are the coordinates of stations i and j, respectively, then the distance between stations, as measured along the direction of propagation of the wave and needed to compute the phase velocity, is computed as follows:

$$\Delta x = \left|\mathbf{e}_{(ij)}\cdot\left[(x_j-x_i)\mathbf{i}+(y_j-y_i)\mathbf{j}\right]\right| \tag{45}$$

In all the above argument, a rectangular Cartesian coordinate system is implied, with the x-axis pointing to the East direction, and the y-axis pointing to the North direction, $\mathbf{i}$ and $\mathbf{j}$ being the unit base vectors defining the positive directions along the x- and y-axes, respectively.

7. Estimation of rotational motions

Having obtained estimates of the phase velocity spectrum of a train of dispersed waves (Rayleigh or Love), we can proceed to

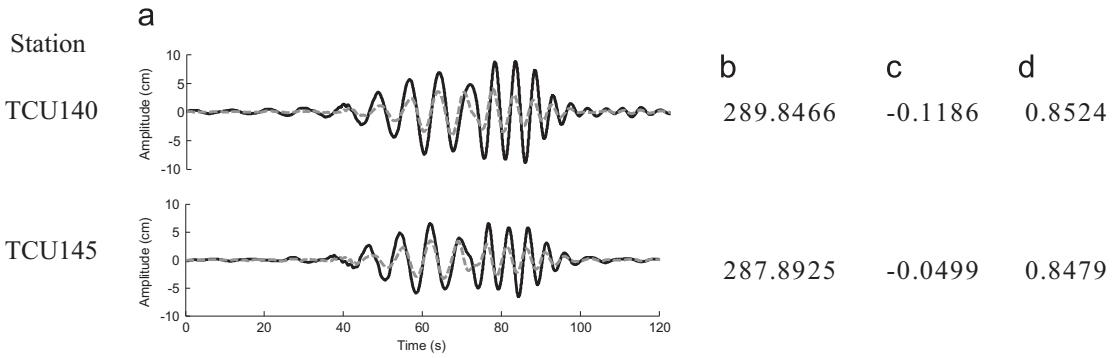

Fig. 19. Extracted Rayleigh waves at stations TCU140 and TCU145. (a) Horizontal component (solid line) and vertical component shifted with a $\pi/2$ phase delay (dashed line). (b) Azimuth of direction of propagation (deg), (c) correlation coefficient between x_{POL} and x_{NRM} components, C_{PN}, and (d) correlation coefficient between x_{POL} and phase delayed vertical components, $C_{P\bar{v}}$.

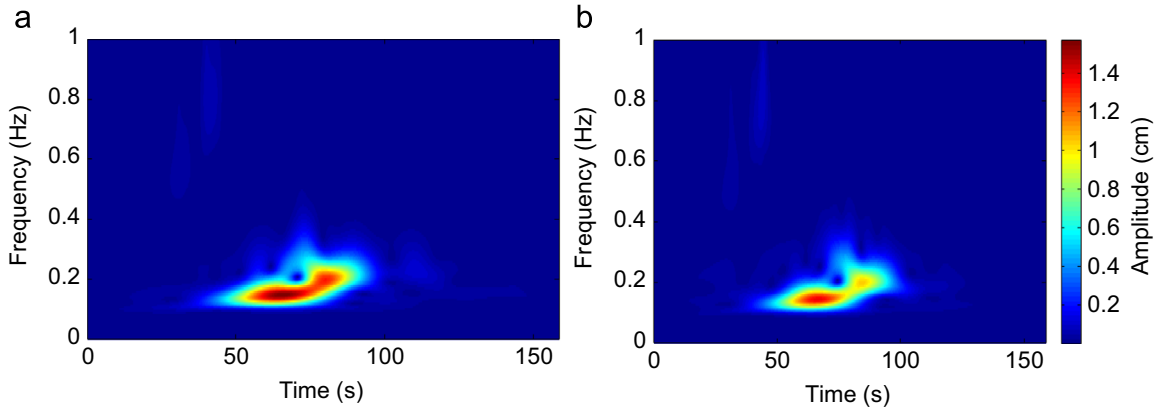

Fig. 20. Amplitude of Transform S_V of extracted Rayleigh waves at (a) station TCU140, (b) station TCU145.

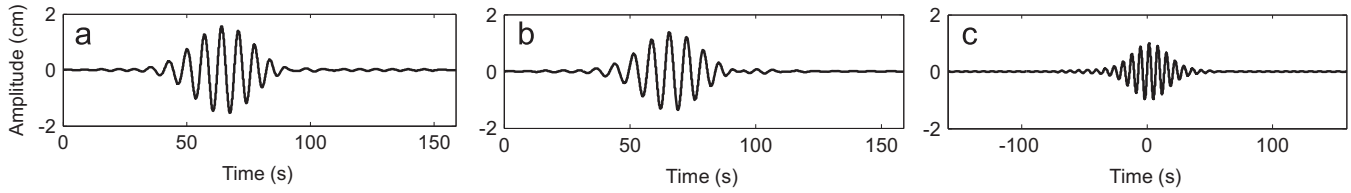

Fig. 21. Shifted voices $S_V(\tau, f_n)\exp(i2\pi f_n t)$ at a frequency $f_n = 0.15$ Hz. (a) Station TCU140 (b) station TCU145 (c) cross-correlation of the two shifted voices.

estimate rotational motions for each 'voice' individually (Eqs. (35) and (36) and then synthesize all the 'voices' (i.e. invert the S-Transform) to obtain the rotational motions in the time domain. We can compare these estimates of rotational motions with the estimates obtained by approximating the displacement gradients (Eqs. (31) and (32)) with finite differences of the appropriate displacement components recorded at the neighboring stations. In order to demonstrate the application of the above procedure we consider two sets of well recorded data: (1) recordings of an aftershock of the 1999 Chi-Chi, Taiwan earthquake which are dominated by Rayleigh waves and induce significant rocking motions; and (2) recordings of the 2010 Darfield, New Zealand earthquake which are dominated by Love waves and induce significant torsional motions.

7.1. Estimation of rocking

In this section we compute rocking associated with Rayleigh waves generated by an aftershock of the Chi-Chi earthquake in the West Coastal Plain (WCP) in Taiwan, which occurred on September, 20th 1999 at 1803 UTC, with a magnitude of Mw 6.2. The Rayleigh waves and their directions of propagation were extracted using the procedure described in the previous sections. Fig. 9 shows a map with the locations of the stations to be considered. We describe in detail the computations of rocking associated with the motions recorded at stations TCU140 and TCU145. The distance Δx between stations in the average direction of propagation is 3.2419 km. The extracted retrograde Rayleigh waves at stations TCU140 and TCU145 are shown in Fig. 19. We can observe a high degree of correlation between the waveforms recorded at the two stations, as expected for a wave train passing under two neighboring stations. At each station the horizontal component is plotted and compared with the vertical component, the latter having been shifted with a $\pi/2$ phase delay. The correlation coefficients between the components of the extracted waves that are also shown in Fig. 19, provide additional evidence that the extracted waves are polarized as Rayleigh waves.

After making sure that the time histories of the extracted waves have the same time origin, we proceed to compute the Stockwell Transform of the vertical component for each station. Their amplitudes are shown in Fig. 20. We can observe the similarity is high between the two transforms. As expected, the wave energy at station TCU145 is lower, since this station is at a greater distance from the vicinity of the basins' edge (on the east of the station)

where the surface waves are generated. A more detailed comparison can be made by inspecting and comparing the "shifted voices" $S_V(\tau,f_n)\exp(i2\pi f_n\tau)$ for the two stations at a frequency $f_n=0.15$ Hz, shown in Fig. 21. In Fig. 21(c) we present the cross-correlation of the two shifted voices, where its maximum is indicated by the black circle. The time corresponding to that maximum gives us the *time-lag* for the 0.15 Hz waves, which for this example is 1.6050 s. Dividing the distance Δx by this time-lag we obtain that the phase velocity for the wave of 0.15 Hz is 2.02 km/s. With this value (which we obtain by correlating the 'voices' of a particular frequency at two stations in the time domain) we confirm the phase velocity we compute using the cross-spectrum of the Stockwell Transforms.

The amplitude of the cross-spectrum $A_{CS}(\tau,f)$ is shown in Fig. 22(a) and its phase $\Phi_{CS}(\tau,f)$ is shown in Fig. 22(b). It is clear that in the region with high amplitude of the cross-spectrum, its phase has an almost constant value. Then the phase velocity spectrum $c_R(f)$ for the Rayleigh waves is computed as given in Eq. (41) and plotted in Fig. 23. We show the phase velocity variation within the frequency range 0.1–0.25 Hz, because those are the frequencies that are highly correlated as indicated by the amplitude of the cross-spectrum $A_{CS}(\tau,f)$. The black dot indicates the phase velocity of 2.02 km/s we computed for the frequency of 0.15 Hz using the cross-correlation of the shifted 'voices'. We can observe that the results obtained with such procedure and with the use of Eq. (41) give the same values for the phase velocity of the extracted waves. We can also observe a sudden change in the phase velocity slope at about 0.17 Hz. We argue that this change is due to the fact that the extracted wave is composed of two dispersive wave trains, with the wave train of higher frequencies traveling at lower phase velocities, as is visually evident from Fig. 20(a) and (b).

Once the phase velocity spectrum is computed, the time history of rocking is obtained by inverting the function $S_\psi(\tau,f_n)$ given in Eq. (35). The resulting rocking histories are shown in Fig. 24. We also plot the rocking history in Fig. 24(c) estimated by the finite difference approximation:

$$\psi(t) = \frac{\partial v}{\partial x} \cong \frac{v_j - v_i}{\Delta x} \tag{46}$$

where Δx in the above expression is distance measured along the (average) direction of propagation; v_i and v_j are the displacement components measured at the two stations i and j, respectively, along the (average) direction of propagation of the wave under consideration. We can observe in Fig. 24 that the rocking motions obtained with our time–frequency procedure, are very similar to the approximation given by Eq. (46).

Following the same steps as above, we estimate rocking from the recordings of another pair of stations located in the WCP, specifically stations TCU118 and TCU112. Fig. 26 displays the rocking time histories for the latter pair of stations using both the cross-spectrum approach as well as the displacement gradient approximated by finite differences. The distance between stations along the average direction of propagation Δx is 4.136 km. Considering that the phase velocity corresponding to a frequency of ~0.20 Hz is ~2.0 Km/sec, we estimate a wavelength of 10.0 km which is two times the computed distance , and thus, sufficient for our strain calculations. The horizontal and shifted vertical components of the extracted Rayleigh waves are shown in Fig. 25, to illustrate the similarity of their waveforms. Once more, Fig. 26 shows that the results we obtain with the time–frequency synthesis for rocking are similar to those obtained using the finite difference approximation.

7.2. Estimation of torsion

In this section, we estimate torsion induced by the Love waves generated by the 2010 Darfield event. First we consider stations PPHS and SMTC. Their waveforms can be compared by inspecting Fig. 7. The distance between the stations in the average direction of propagation is 2.357 km. The amplitude of the Stockwell Transform cross-spectrum is displayed in Fig. 27(a) and the calculated phase velocity spectrum for Love waves in Fig. 27(b). The cross-spectrum shows that the time of highest correlation between the Love waves is before 50 s. With the phase velocity of Fig. 27(b) we compute the torsional motions using Eq. (36). The resulting torsion histories are presented in Fig. 28, and once again, they appear to be in excellent agreement with the estimations obtained by the finite difference approximation shown in Fig. 28 (c). A similar conclusion can be made for the torsion estimated at stations CBGS and REHS, shown in Fig. 29. For this pair of stations $x=1.9074$ km, and the displacements histories were low-pass

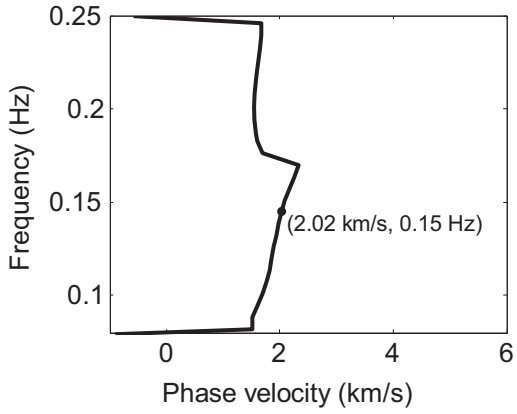

Fig. 23. Phase velocity spectrum for extracted Rayleigh waves.

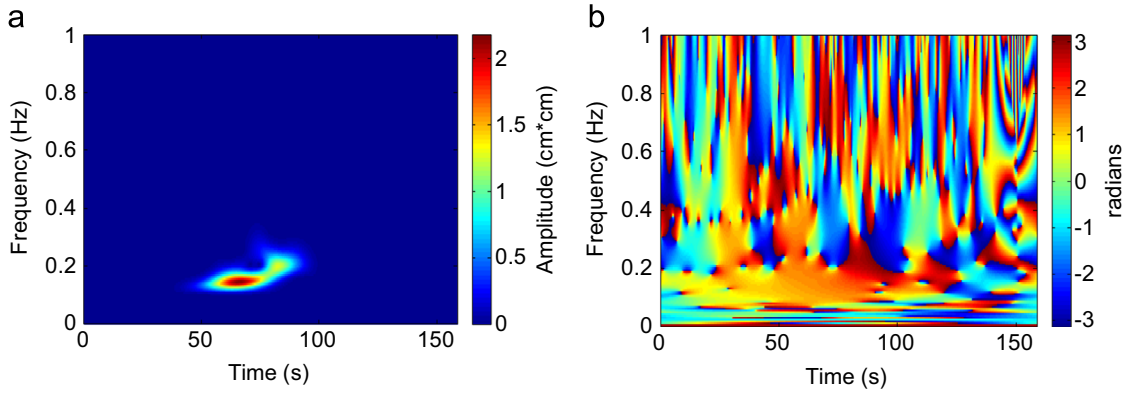

Fig. 22. Cross-spectrum of Stockwell Transforms of extracted Rayleigh waves at stations TCU140 and TCU145 (a) amplitude, and (b) phase.

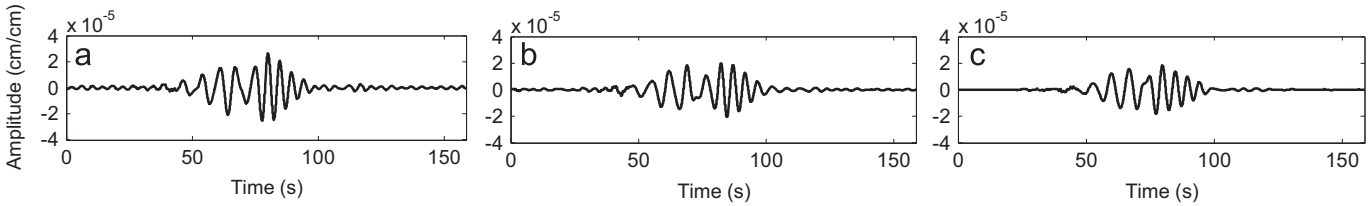

Fig. 24. Rocking histories (a) at station TCU140, (b) at station TCU145, and (c) computed with finite difference approximation.

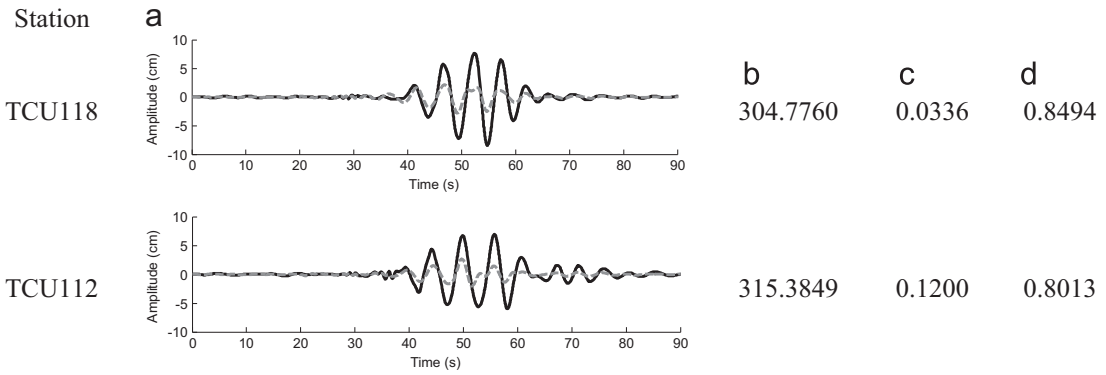

Fig. 25. Extracted Rayleigh waves at stations TCU118 and TCU112. (a) Horizontal component (solid line) and vertical component shifted with a $\pi/2$ phase delay (dashed line). (b) Azimuth of direction of propagation (degrees), (c) correlation coefficient between x_{POL} and x_{NRM}. components, C_{PN}, and (d) correlation coefficient between x_{POL} and phase delayed vertical components, $C_{P\bar{v}}$.

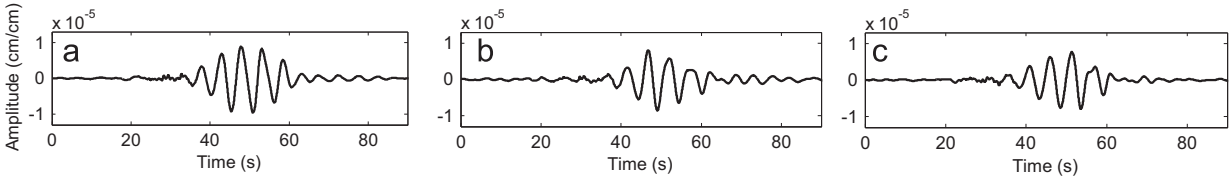

Fig. 26. Rocking histories (a) at station TCU118, (b) at station TCU112, (c) computed with finite difference approximation.

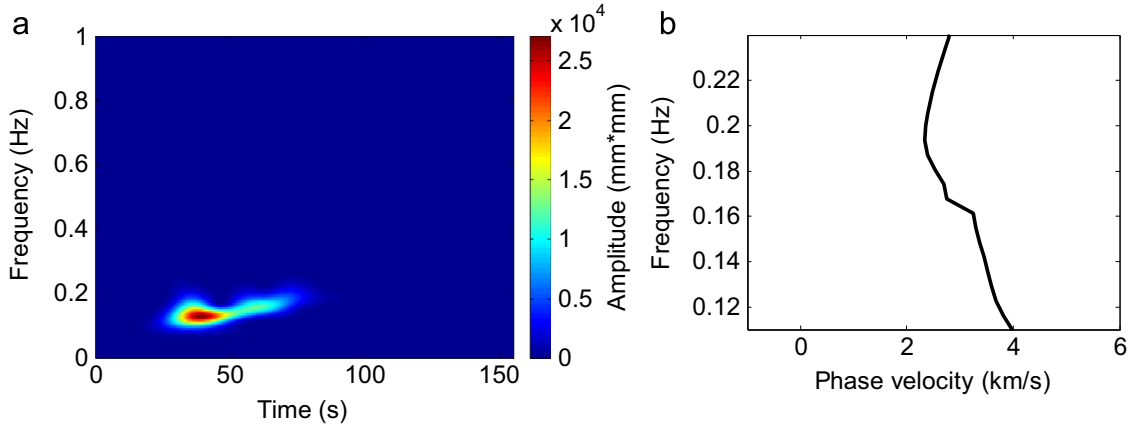

Fig. 27. (a) Cross-spectrum of Stockwell Transforms of extracted Love waves at stations PPHS and SMTC and (b) phase velocity spectrum for extracted Love waves.

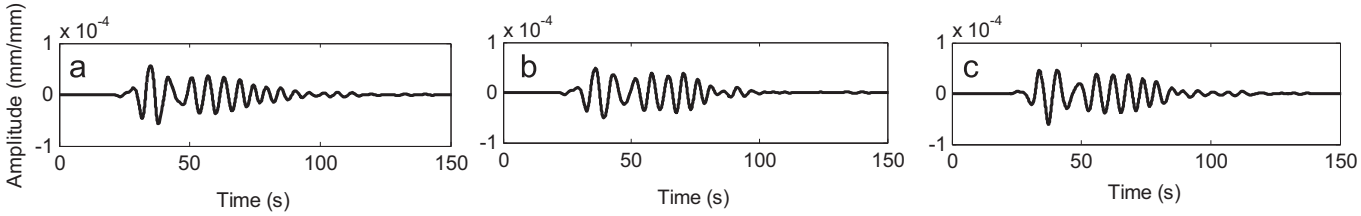

Fig. 28. Torsion histories (a) at station PPHS, (b) at station SMTC, and (c) computed with finite difference approximation.

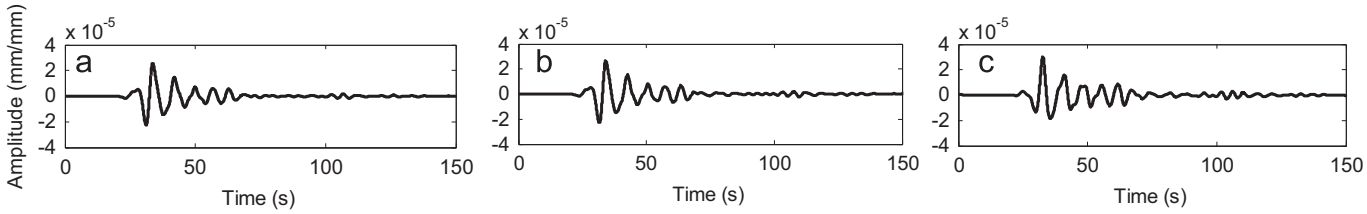

Fig. 29. Torsion histories (a) at station CBGS, (b) at station REHS, and (c) computed with finite difference approximation.

filtered with a cut-off frequency of 0.22 Hz to remove the high-frequency noise. Since for stations CBGS and REHS the relevant (dominant) frequency appears to be 0.15 Hz and the relevant velocity appears to be about 2.5 km/s, the wavelength is estimated as 16.7 km, which is over six times larger than the reported distance and consequently accurate enough to compute strains. Even though we observe less dispersion in this case, we consider the extracted waves as being Love waves, because the direction of polarization (as indicated in Fig. 7) is perpendicular to the direction of propagation.

8. Conclusions

We have applied a technique for identifying and extracting surface waves (Rayleigh and Love waves) exploiting their polarization characteristics and using as tool the Stockwell Transform (S-Transform). This technique, originally proposed in Meza-Fajardo et al. [14], has been somewhat refined and improved for extracting Love waves in the present work. Also, if the seismic motion has been recorded by stations that are sufficiently close, then the S-Transform makes it feasible to calculate the phase velocity spectrum of the surface wave train that has been extracted. This spectrum can subsequently be used in a straightforward calculation to evaluate rotational motions, such as rocking and torsion. The proposed technique of identifying and extracting surface waves (Rayleigh and/or Love) is a necessary first step in computing rotational motions from a given recording of translational motions. Specifically, we need to separate the body waves from the surface waves in order for each set of wave train to compute the associated rotational motions because, as is well known, body waves are not dispersed (and therefore c_{app} is frequency independent in Eqs. (31) and (32)) while surface waves are dispersed and $c_{app} = c_{R,L}(\omega)$ is frequency dependent.

9. Data and resources

The seismograms of the 1999 Chi-Chi earthquake used in this work are from CD-002 titled “CWB Free-Field Strong-Motion Data from three Major Aftershocks of the 1999 Chi-Chi earthquake: Processed Acceleration Data Files on CD-ROM” prepared in 2001 by W.H.K. Lee, T.C. Shin, and C.F. Wu of the Seismological Observation Center, Central Weather Bureau, Taiwan.

All displacements histories corresponding to the 2010 Darfield event in New Zealand were retrieve from the Strong-Motion Database of the GeoNet website, the official source of geological hazard information for New Zealand. The seismograms were accessible through the address: ftp.geonet.org.nz/strong/processed/Proc.

The relief geographic map of the West Coastal Plain was generated with the code READHGT written by François Beauducel, from the Institute de Physique du Globe de Paris. Input data for the Digital Elevation Map was downloaded from http://dds.cr.usgs.gov/srtm/version2_1. Coast lines were extracted from http://www.ngdc.noaa.gov/mgg/coast/getcoast.html.

All the websites mentioned above were last accessed in March 2015.

Acknowledgments

This research has been financed by the European Union (European Social Fund – ESF) and Greek national funds through the Operational Program "Education and Lifelong Learning" of the National Strategic Reference Framework (NSRF 2007-2013) - Research Funding Program: **THALES**. Investing in knowledge society through the European Social Fund.

Appendix A

In order to make the presentation easier to follow, we briefly present the definition of the S-Transform, $S_h(\omega)$, of a give signal $h(t)$ [16,17] and its inverse (in order to recover the original signal from the S-Transform), writing symbolically: $h(t) \overset{S}{\leftrightarrow} S_h(\omega)$. Then, we proceed to demonstrate how Eqs. ($S_\psi(\tau,\omega)$, $S_\varphi(\tau,\omega)$) follow from Eqs. ($\tilde{\psi}(\omega)$, $\tilde{\varphi}(\omega)$). The S-transform (ST) produces a time–frequency representation of a time series. It is a generalization of the short-time Fourier transform (STFT), extending the continuous wavelet transform (CWT) and overcoming some of its disadvantages. It is based on a moving and scalable localizing Gaussian window. We start with the definition of the S-Transform:

$$S_h(\tau,f) = \int_{-\infty}^{+\infty} h(t)\left\{\frac{|f|}{\sqrt{2\pi}} e^{-f^2(\tau-t)^2/2}\right\} e^{-i2\pi f t} dt \tag{A.1}$$

It is straightforward to demonstrate that the inverse S-Transform is given by:

$$h(t) = \int_{-\infty}^{+\infty} \left[\int_{-\infty}^{+\infty} S_h(\tau,f) d\tau\right] e^{i2\pi f t} df \tag{A.2}$$

If $\tilde{h}(\omega)$ (where $\omega = 2\pi f$) is the Fourier transform of $h(t)$, symbolically $h(t) \overset{\mathcal{F}}{\leftrightarrow} \tilde{h}(\omega)$, then it follows that:

$$\int_{-\infty}^{+\infty} S_h(\tau,f)\, d\tau = \tilde{h}(\omega) \tag{A.3}$$

The 1-D function of time for a given frequency $f = f_n$, which shows how the amplitude and phase for this exact frequency changes over time is referred to as the ‘*voice*’ of frequency f_n and is written as $S_h(\tau,f_n)$. The ‘voice’ in essence is obtained from the original signal, $h(t)$, by band-pass filtering, the filter being the Gaussian function. The function $\hat{h}(t) = 2 \cdot S_h(t,f_n) e^{i2\pi f_n t}$, $(f_n > 0)$ is referred to as the ‘*analytic signal*’.

In Eq. ($S_\psi(\tau,\omega)$) we argued that the ‘voice’ for rocking is given by the expression $\left(\frac{i\omega}{c_R(\omega)}\right) \cdot S_w(\tau,\omega)$. This implies that if we apply the inverse S-Transform to this quantity we should recover $\psi(t)$. Indeed,

$$\int_{-\infty}^{+\infty} \left[\int_{-\infty}^{+\infty} \left(\frac{i2\pi f}{c_R(2\pi f)}\right) \cdot S_w(\tau,f)\, d\tau\right] e^{i2\pi f t}\, df$$

$$
\begin{aligned}
&= \int_{-\infty}^{+\infty} \left(\frac{i2\pi f}{c_R(2\pi f)}\right) \cdot \left[\int_{-\infty}^{+\infty} S_w(\tau, f)\, d\tau\right] e^{i2\pi f t}\, df \\
&\overset{\omega = 2\pi f}{=} \frac{1}{2\pi} \int_{-\infty}^{+\infty} \left(\frac{i\omega}{c_R(\omega)}\right) \cdot \tilde{w}(\omega) \cdot e^{i\omega t}\, d\omega \\
&= \frac{1}{2\pi} \int_{-\infty}^{+\infty} \tilde{\psi}(\omega) \cdot e^{i\omega t}\, d\omega \\
&= \psi(t)
\end{aligned}
\tag{A.4}
$$

Similarly we can demonstrate that the 'voice' for torsion is given by the expression $-\left(\frac{1}{2}\right)\left(\frac{i\omega}{c_L(\omega)}\right) \cdot S_v(\tau, \omega)$.

References

[1] Bouchon M. The motion of the ground during an earthquake - 1. The case of a strike slip fault. J Geophys Res 1980;85(B1):356–66.

[2] Bouchon M, Aki K. Strain, tilt and rotation associated with strong ground motion in the vicinity of earthquake faults. Bull Seismol Soc Am 1982;72 (5):1717–38.

[3] Bycroft GN. Soil-foundation interaction and differential ground motions. Earthq Eng Struct Dyn 1980;8(5):397–404.

[4] Castellani A, Boffi G. Rotational components of the surface ground motion during an earthquake. Earthq Eng Struct Dyn 1986;14:751–67.

[5] Castellani A, Boffi G. Rotational components of seismic motion. Earthq Eng Struct Dyn 1989;18:785–97.

[6] Ferrari G. Note on the historical rotation seismographs, in earthquake source asymmetry. In: Teisseyre R, Takeo M, Majewski E, editors. Structural media and rotation effects. Heidelberg: Springer-Verlag; 2006. p. 367–76.

[7] Gomberg J. Dynamic deformations and M 6.7, Northridge, California earthquake. Soil Dyn Earthq Eng 1997;16(7–8):471–94.

[8] Hart GC, DiJulio M, Lew M. Torsional response of high-rise buildings. J Struct Div ASCE 1975;101:397–414.

[9] Huang B-S. Ground rotational motions of the 1999 Chi-Chi, Taiwan earthquake as inferred from dense array observations. Geophys Res Lett 2003;30(6):1307. http://dx.doi.org/10.1029/2002GL015157.

[10] Loh C-H. Analysis of the spatial variation of seismic waves and ground movements from SMART-1 array. Data Earthq Eng Struct Dyn 1985;13:561–81.

[11] Luco JE. Torsional response of structures to obliquely incident seismic SH waves. Earthq Eng Struct Dyn 1976;4:207–19.

[12] Luco JE, Sotiropoulos DA. Local characterization of force-field ground motion and effects of wave passage. Bull Seismol Soc Am 1980;70:2229–44.

[13] Malvern LE. Introduction to the mechanics of a continuous medium. Englewood Cliffs, New Jersey: Prentice-Hall; 1969.

[14] Meza-Fajardo KC, Papageorgiou AS, Semblat JF. Identification and extraction of surface waves from three-component seismograms based on the normalized inner product. Bull Seismol Soc Am 2015;105(1):210–29.

[15] Newmark NM. Torsion in symmetrical buildings. In: Proceedings of the 4th world conference on earthquake engineering. Chile: Universidad de Chile Santiago; 1969.

[16] Stockwell RG, Mansinha L, Lowe R. Localization of the complex spectrum: the S transform. IEEE Trans Signal Process 1996;44(4):998–1001.

[17] Stockwell RG. Why use the S-transform, in pseudo-differential operators: PDEs and time–frequency analysis. In: Wong A, editor. (Fields Institute Communications), Vol. 52. Providence, Rhode Island: American Mathematical Society (AMS); 2007. p. 279–309.

[18] Trifunac MD. A note on rotational components of earthquake motions for incident body waves. Soil Dyn Earthq Eng 1982;1(1):11–9.

[19] Trifunac MD. Review: rotations in structural response. Bull Seismol Soc Am 2009;99(2B):968–79.

[20] Trifunac MD, Todorovska MI, Ivanovic SS. Peak velocities, and peak surface strains during Northridge, California, earthquake of 17 January 1994. Soil Dyn Earthq Eng 1996;15(5):301–10.

[21] Zembaty Z. Tutorial on surface rotations from wave passage effects: stochastic spectral approach. Bull Seismol Soc Am 2009;99(2B):1040–9.